ITR-1528

PRELIMINARY REPORT

OPERATION PLUMBBOB

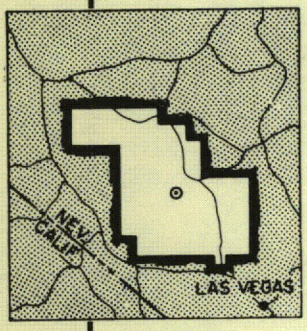

NEVADA TEST SITE
MAY-OCTOBER 1957

Project 26.4a

SURFACE MOTION FROM AN UNDERGROUND DETONATION

Issuance Date: February 28, 1958

UNIVERSITY of CALIFORNIA RADIATION LABORATORY
LIVERMORE, CALIFORNIA

NOTICE

This report is published in the interest of providing information which may prove of value to the reader in his study of effects data derived principally from nuclear weapons tests.

This document is based on information available at the time of preparation which may have subsequently been expanded and re-evaluated. Also, in preparing this report for publication, some classified material may have been removed. Users are cautioned to avoid interpretations and conclusions based on unknown or incomplete data.

PRINTED IN USA
Price $1.75. Available from the Office of
Technical Services, Department of Commerce,
Washington 25, D. C.

AEC Technical Information Service Extension
Oak Ridge, Tennessee

ITR-1528

Operation PLUMBBOB Preliminary Report

Project 26.4a

SURFACE MOTION FROM AN UNDERGROUND DETONATION

By

L. M. Swift, D. C. Sachs, J. L. Brenner and W. M. Wells

Stanford Research Institute
Menlo Park, California

October 15, 1957

ABSTRACT

Surface and near-surface acceleration and strain were measured on a deep underground nuclear burst (Rainier Shot; 900 ft; 1.7 kt) to permit extrapolation of results to nuclear detonations of other yields under different test or employment conditions.

Results indicate that a large earth cap, beginning approximately 180 ft below the mesa surface, separated from the mesa over the charge and subsequently fell back into place. The only significant vertical displacement occurred at or near ground zero and reached a maximum of 1 ft. Both acceleration and horizontal strain measurements suggest that the principal disturbance on the mesa surface was confined to a small region around ground zero.

From preshot seismic survey data and Rainier gage arrival times and average vertical strains it is concluded that the medium was many-layered with seismic velocities which were widely different in the various layers.

These conclusions resulted from a preliminary analysis of the data; for the final report, more exacting analysis will be undertaken as outlined at the end of this report.

ACKNOWLEDGMENT

The authors wish to acknowledge the excellent cooperation and guidance of Dr. R. G. Preston, director, Program 26, and Mr. D. T. Schueler Jr., of his staff. The effective assistance of Mr. J. M. Polatty of Waterways Experiment Station, in design and execution of instrument grouting methods, is also gratefully acknowledged.

The planning and execution of Project 26.4a were under the direction of Mr. L. M. Swift with Mr. W. Wells serving as field supervisor and Mr. L. H. Inman as field party chief. Other members of the field party included V. E. Krakow, C. M. Westbrook, R. V. Ohler, H. C. Wuner and R. E. Aumiller. Dr. D. C. Sachs, Dr. J. L. Brenner, Miss Diane Smithem, Miss Sherry Ward, and Miss Phyllis Flanders assisted in the data analysis and technical preparation of this report.

CONTENTS

CONTENTS (cont)

TABLES

FIGURES

CHAPTER 1

INTRODUCTION

1.1 OBJECTIVES

Program 26, associated with Shot Rainier (a deep underground detonation) at the Nevada Test Site, had as its general objective the development of sufficient data on earth motion (i.e., acceleration, strain, and displacement in the medium and on the surface and seismic disturbances on the surface) to permit extrapolation of the test results to nuclear detonations of other yields and under different test or employment conditions.

Specifically, the objective of Project 26.4a was to obtain data on the surface and near-surface earth motions produced by Shot Rainier, a 1.7-kt charge detonated approximately 900 ft below the ground surface.

1.2 BACKGROUND

Rainier shot was designed to examine the feasibility of using underground shots for diagnostic testing of nuclear devices. The location chosen for Rainier was in Area 12 under the mesa forming the northwestern boundary of Yucca Flat. The material of the mesa was volcanic tuff, with a specific gravity of 1.6 to 1.9, overlain by a cap of rhyolite (welded tuff) from 200 to 300 ft thick. (Reference 1 presents a more detailed description of the geology of the mesa; see also Appendix A of this report.)

The chief criterion for the proposed use of underground detonations is that the shot be "contained," that is, that it produce no appreciable offsite fallout. Unfortunately, very little applicable experimental data existed with which to determine the depth required for containment of a 1.7-kt charge in the material selected. Not only was there a dearth of data, but scaling of predictions over a wide range of yields leaves much to be desired, as is evident in a study of crater formation from shallow shots (Reference 2).

A great amount of information was available on the containment of relatively small high-explosives detonations in common soils and in rock formations; but the former was not applicable to the medium of Area 12, and the latter was questionable because of the effects of "tamping" with other than original materials. Little pertinent data were to be had from the several large high-explosives shots conducted by the Corps of Engineers at moderate scaled depths in limestone, granite, and sandstone during their Underground Explosions Tests (1951) since none of these was deep enough to be completely contained (Reference 3).

In Nevada, only two previous underground nuclear shots had been detonated: Jangle U and Teapot Ess (Shot 7), each with a yield of 1.2 kt and with

charge burial depth of 17 and 67 ft, respectively (references 4 and 5). They were shot in the loosely cemented conglomerate of floor of Yucca Flat, not in the mesa tuff. Both shots produced large craters but not as large as had been generally predicted.

In view of the sparse background information on the characteristics of deep underground detonations in rock, it was decided to detonate two high-explosives shots (10 and 50 tons) in a tuff formation a few miles from Rainier site to aid in the predictions for the Rainier shot. These shots were at lesser scaled depths than Rainier, and both may be considered to have been contained although pronounced surface effects were observed (reference 6).

CHAPTER 2

EXPERIMENT PLAN

2.1 ACCELERATION AND STRAIN MEASUREMENTS

Station layout is shown in Fig. 2.1 and Table 2.1. For an idealized view of the experiment plan, see inset, sketch A. (A, S designate acceleration and strain measurements.)

Vertical acceleration was measured at 0, 100, 180, 250, and 320 ft below the mesa surface in a 350 ft hole over ground zero and at several ground ranges on the mesa surface and slope. Horizontal acceleration in the radial plane was measured at several surface ground ranges and at all but one station, that opposite ground zero, on the mesa slope.

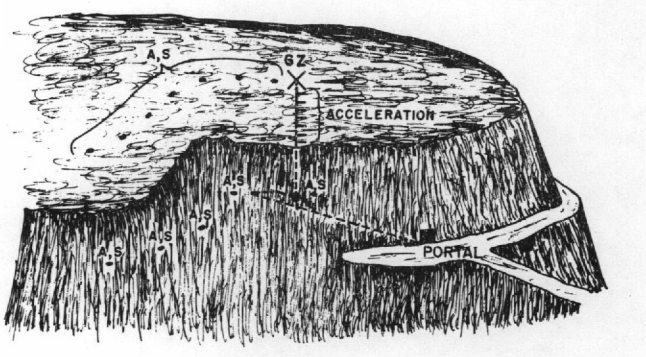

Sketch A

Transverse strain was measured on the surface only at approximately 650 and 900 ft from ground zero. Horizontal radial strain was measured at approximately 0, 650, 900, and 1900 ft on the surface and at approximate mately 0 and 400 ft on the slope. (Although the nomenclature for gages on this project indicates that one of the two strain gages at ground zero on the mesa surface is measuring transverse strain, in reality it is measuring horizontal strain since its reference point is the same as that for the horizontal strain gage and is located over ground zero, see sketch B at left)

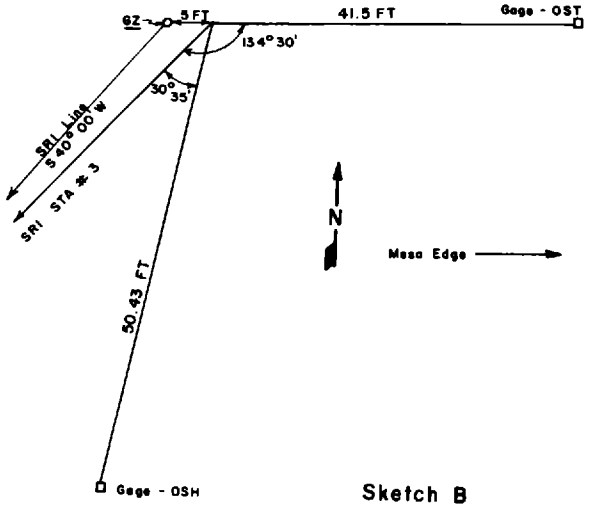

Sketch B

As shown in Fig. 2.1, Stations 0 through 6 were on the mesa surface, Stations 10 through 13 on the slope. The deep hole (Sta 0) was drilled as close to ground zero as was practical, and the remaining mesa stations were laid out in a southerly direction from ground zero. The latter were placed at lease 300 ft from the edge of the mesa to avoid any disturbances caused by jointing or planes of weakness in the rhyolite cap. Stations 10 through 13 were located at four positions on the face of the slope where the granular tuff was exposed just below the rhyolite-tuff interface. Stations 3 and 4 were jointly occupied by U.S. Coast and Geodetic Survey (USC & GS) and Stanford Research Institute (SRI).

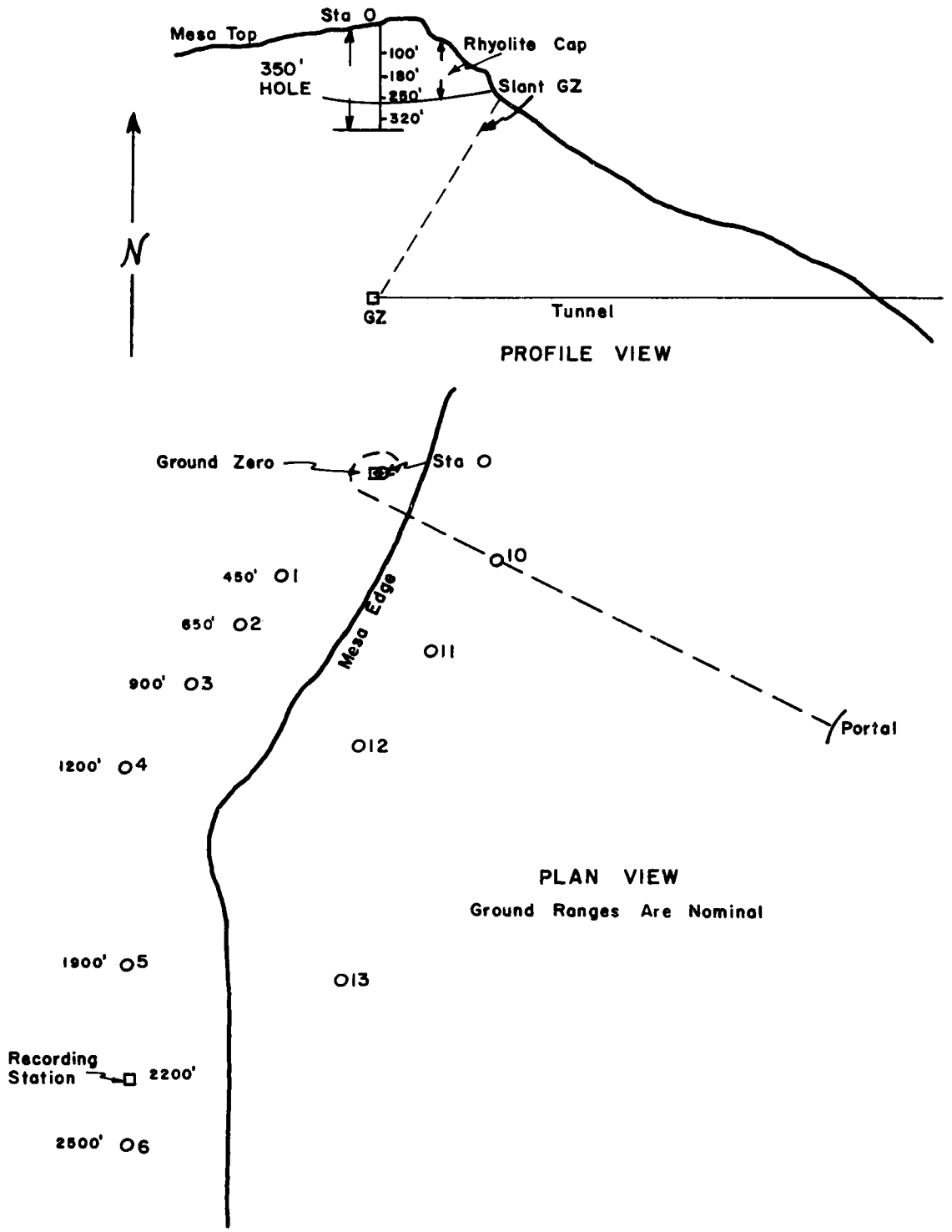

Fig. 2.1 Station layout

TABLE 2.1 GAGE LAYOUT

Nominal ground range, ft	Station No. and Gage code	Gage rating	Predicted peak	Type galvanometer, Standard - A
0	0AP 0	5 g	1.5-3.0 g	3-3
Deep hole	0AP 100'	5 g	2.0 g	3-2
Deep hole	0AP 180'	5 g	3.0 g	3-2
Deep hole	0AP 250'	10 g	5.0 g	3-2
Deep hole	0AP 320'	10 g	6.6 g	3-2
	0SH	50.43' span	+ 5 ppk	3-3
	0ST	41.5' span	+ 5 ppk	3-3
450	1AP	5 g	1.1 g	3-2
	1AH	1 g	0.30 g	3-3
650	2AP	1 g	0.9 g	3-3
	2AH	1 g	0.3 g	3-3
	2SH	51.1' span	+ 1.3 ppk	3-3
	2ST	54.6' span	+ 4.0 ppk	3-3
900	3AP	1 g	0.8 g	3-3
	3AH	1 g	0.3 g	3-2
	3SH	62.3' span	- 1.0 ppk	3-3
	3ST	47.68' span	+ 1.8 ppk	3-3
1250	4AP	1 g	0.6 g	3-3
	4AH	1 g	0.3 g	3-3
	4SH	100.25' span	- 0.8 ppk	3-3
1900 (1795)*	5AP	1 g	0.4 g	3-3
	5AH	1 g	0.25 g	3-3
	5SH	92.9' span	- 0.6 ppk	3-3
2500 (2340)*	6AP	1.g	0.35 g	3-3
	6AH	1 g	0.25 g	3-3
0	10AP	5 g	2.0 g	3-3
	10SH	66.3' span	+ 8.0 ppk	3-3
400(±)	11AP	5 g	1.2 g	3-3
	11AH	1 g	0.5 g	3-3
	11SH	38.25' span	+ 2.5 ppk	3-3
800(±)	12AP	1 g	0.75 g	3-3
	12AH	1 g	0.4 g	3-3
1500(±)	13AP	1 g	0.5 g	3-3
	13AH	1 g	0.3 g	3-3

* Straight line distance from ground zero. (Stations 0-6 on mesa - range from mesa ground zero; stations 10-13 on slope - range approximately from slant ground zero.)

Predicted peaks for acceleration are measured in multiples of force of gravity, g, and for strain in parts per thousand, ppk.

2.2 PREDICTIONS

To select gage ranges and attenuator settings, it is necessary to predict the magnitude of phenomena resulting from the detonation. These predictions, however, are approached with a somewhat different attitude from that of analyses which are intended to evaluate the underground experiment as a whole or which are intended to develop a prediction technique. The approach is highly empirical and is colored by intuition based on experience and judgment of the quality of available data. A conscious effort was made to avoid the general tendency to over-predict effects, which has historically marred the effectiveness of projects associated with nuclear explosions, particularly underground explosions.

Predictions used for range settings were based largely on direct scaling of phenomena measured on the U. S. Geological Survey (USGS) 50-ton shot (Reference 6) and on the Underground Explosion Tests (UET) in Utah Sandstone (Reference 3). These tests were conducted in media resembling reasonably well the medium of Rainier site; Jangle U and Teapot Ess (Shot 7) were in a medium differing from that of Rainier and can be considered only for guidance in selecting lower limits of range settings.

2.2.1 HE Equivalence. The yield of a nuclear explosion is customarily stated in terms of the equivalent weight of TNT which would produce the same total energy release. In an aboveground nuclear explosion, it is well established that the mechanical (blast) effects are less than and other effects (thermal radiation, for instance) are greater than those produced by the corresponding amount of TNT. The HE efficiency of an aboveground nuclear explosion for airblast is about 46 percent; that is, a 1-kt device will produce the same blast effects as 0.46 kt of TNT.

The HE efficiency of an underground nuclear explosion for underground phenomena is not as well established. It is affected by a number of factors: the air space around the device, the density, heat of melting, and heat of vaporization of the medium, and the water content of the medium, and the mass-to-yield ratio of the device, especially for small yields. Because of scaling problems, it has been difficult to define the HE efficiency of the two previous underground nuclear bursts in terms of all observed dynamic phenomena. However, calculations based on dynamic phenomena and on crater radius and volume suggest an HE efficiency for underground explosions of from 25 to 40 percent.

To be conservative, an HE efficiency of 40 percent was chosen for direct predictions for this project. This corresponds to an assumed HE equivalent of 0.72 kt, or 1.44×10^6 lb of TNT.

2.2.2 Scaling Laws. For close-in phenomena, it is assumed that "cube-root" scaling holds; i.e., that observed phenomena at equivalent scaled ranges ($R/W^{1/3}$) may be scaled appropriately to any size shot in the same or a similar medium. This is assumed to hold directly for peak strain or particle velocity. Since the time factors change directly as $W^{1/3}$, scaled peak accelerations will vary inversely, and displacements directly, as $W^{1/3}$.

Direct scaling can be expected to apply only when all factors of geometry are scaled. At considerable distances from ground zero, and near the surface,

reflections and refractions of energy may affect the phenomena markedly; in addition it is important to consider differences in scaled charge depth and formation thickness in scaling from one shot to another.

2.2.3 Acceleration. In Reference 3 measured peak radial accelerations are presented from a number of 320-lb and three 40,000-lb HE shots in Utah Sandstone (UET). The latter were at a charge depth of only 12.5 ft (0.365 $W^{1/3}$). The 320-lb charges were at depths ranging from 2.5 (0.365 $W^{1/3}$) to 25 ft (3.65 $W^{1/3}$). Since the 900-ft charge depth of Rainier represents a depth of about 8 $W^{1/3}$, for 0.68 kt (using 40 percent HE energy equivalence) the data from the deepest of these shots were considered the most pertinent, and the best-fit straight line through these data is shown in Fig. 2.2, scaled to Rainier (0.72-kt HE equivalent). Note that the coordinates of the plot are acceleration and distance, rather than ground range.

The USGS 50-ton shot was shot at a depth of 180 ft, a scaled depth of slightly under 4 $W^{1/3}$, but in a medium closely resembling that of the Rainier site. The peak accelerations observed on the surface at several ranges are shown in Table 2.2, as are these values scaled to the Rainier shot. When these points are plotted on Fig. 2.2, it is seen that all but one fall markedly below the scaled UET curve.

TABLE 2.2 50-TON SHOT -- OBSERVED PEAK ACCELERATIONS

Station	Slant range, ft	A_{max}, g	Scales* Slant range	Scaled* A_{max}, g
G0	180	62	438	25.6
B1	223	1	541	0.41
B4	250	1.75	608	0.72
B6	205	8.5	498	3.5

* To Rainier, 720 tons, scale factor 2.43.

For reference, the scaled acceleration-vs-distance curve for Teapot Ess (Shot 7) is also shown on Fig. 2.2; this curve was obtained by direct scaling from 1.2 kt to 1.7 kt. The very low values on this curve represent an absolute lower limit since the medium for this shot was the unconsolidated sand and gravel of Yucca Flat. The change in slope of this curve, however, is typical of data from real explosions which include the effects of the surface and of reflections and refractions from deeper layers. The slope of the curve tends to change from about -4 at short radii to -2 or less at greater radii.

For range setting of channels measuring vertical acceleration, a prediction curve was drawn slightly below the scaled UET line at distances out to 1000 ft, then curving to a slope of about -2 at 3000 ft. On the basis of previous data, horizontal radial accelerations were predicted to be less than vertical, about half at close ranges, rising to about 75 percent at remote ranges.

It should be noted also that although the magnitude of particle velocity in the medium (V) is proportional to stress (S), the direction of V is the

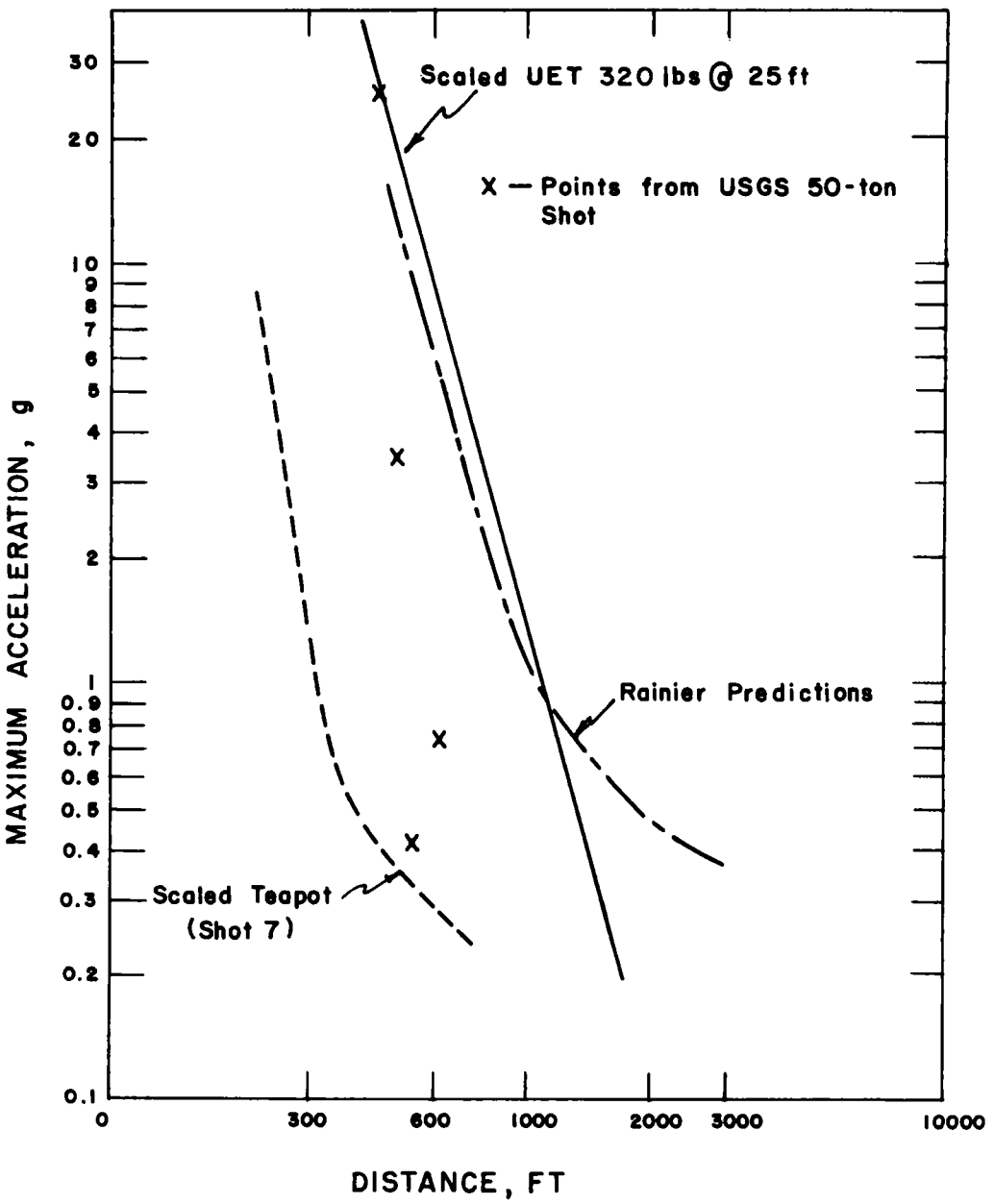

Fig. 2.2 Maximum acceleration vs distance

is the direction of travel of the stress wave. Now, the acceleration is proportional to the stress space gradient, ds/dy, and equal to dv/dt. It is well known that a plane compressive (positive) stress wave upon reflection at a free surface becomes a plane tension (negative) wave in the same direction. Thus, as a consequence of the above relations, a downward-travelling negative stress pulse will cause velocity and acceleration in the same direction as an upward-travelling positive stress pulse. Finally, if ground motion is observed at a depth y between the surface and a source at a greater depth, one would also expect to observe at depth y the influence of the negative stress from the surface reflection.

2.2.4 Strain. The interest of this project in strain was limited to surface strain, as opposed to that in the interior of the medium. As yet, there appears to be no reliable method of tying the two together, except for a reasonable belief that surface strain is greater than that which would be present in the infinite medium if the surface were not present. Without detailing the data, it may be shown that scaling of strain data from the UET shots would predict compressive radial strains of the order of 8 to 20 parts per million at a 900-ft radius from shot Rainier in the semi-infinite medium. This may be taken as a lower limit when surface strain is considered.

The most profitable approach to the prediction of surface strain was considered to be its derivation from predicted displacement. Preliminary reduction of photographic data from the USGS 50-ton shot was reported to show a maximum upward displacement above ground zero of approximately 15 ft. This shot was at a scaled depth of about 4 $W^{1/3}$. Had it been at twice this depth (to correspond to Rainier), this displacement would have been less by a factor of about 8, or 2 ft, assuming slope of -3 of the curve of displacement-vs-slant range. Scaling this assumed displacement of 0.72-kt HE equivalent for Rainier produces a predicted maximum vertical displacement of slightly under 5 ft.

The larger an explosion, the longer the time scale of many of its major phenomena. Duration of positive phase of the pressure pulse is greater for larger explosions, and as a consequence of this, the duration of positive particle velocity, duration of positive displacement phase, and time to return to steady state are all greater. For this reason, the transient stress and displacement have time to adjust themselves more nearly to the values they would have in a stationary problem.

Assuming the medium to behave elastically, the equation of motion, and also the pressure at the shot chamber, are functions of time. There are additional conditions which say that the surface is free from stress, that there is a superimposed gravitational stress field, and that the pressure against the walls of the shot chamber is building up with time. If at the time of maximum displacement, the pressure against the walls of the shot chamber is constant, is equal to its maximum value, and $d^2 \bar{u}/dt^2$ is zero ($\bar{u}$ is the displacement vector), the problem then becomes one of finding the equilibrium (static) position of a large elastic solid under the influence of a buried pressure center. The solution reveals that the surface manifestation of the disturbance will be a pimple directly above the pressure center. In Appendix B, the problem and analytic solution are reproduced from Reference 7.

While the assumption of elasticity is far from accurate, it is believed to give useful results in a real medium. Figure 2.3 shows the calculated variation with radial distance from zero of some of the pertinent parameters, normalized against W_0 (maximum vertical displacement) and S_0 (maximum infinitesimal strain at ground zero). In this figure, it is seen that while the vertical displacement and transverse strain decrease with ground range but never reverse, the radial displacement reached a peak and the radial strain crosses zero at a ground range of 0.707 h, where h is the depth of the charge below the surface. At ground ranges less than this value, the radial strain is tensile; at greater ground ranges, it is compressive.

In the regions where tensile strains were predicted, particularly, it seemed highly probable that the behavior would be inelastic, because of the jointed nature of the surface and near-surface medium. Such joints would not support tensile stress. Moreover, the infinitesimal strains are not expected to be the same for a dynamic problem as for a static one. However, long-span strains should be alike for both the static and the dynamic problems provided the span is sufficiently great. Without arguing the quantitative meaning of "sufficiently great," for prediction purposes it was felt that the general shape of the rise could be predicted well enough from elastic theory and that average strain predictions would be valid. The span (approx. 50 ft) of the strain gages was considered to be long, and the curves of Fig. 2.3 were used for range setting of the strain gages installed on the surface.

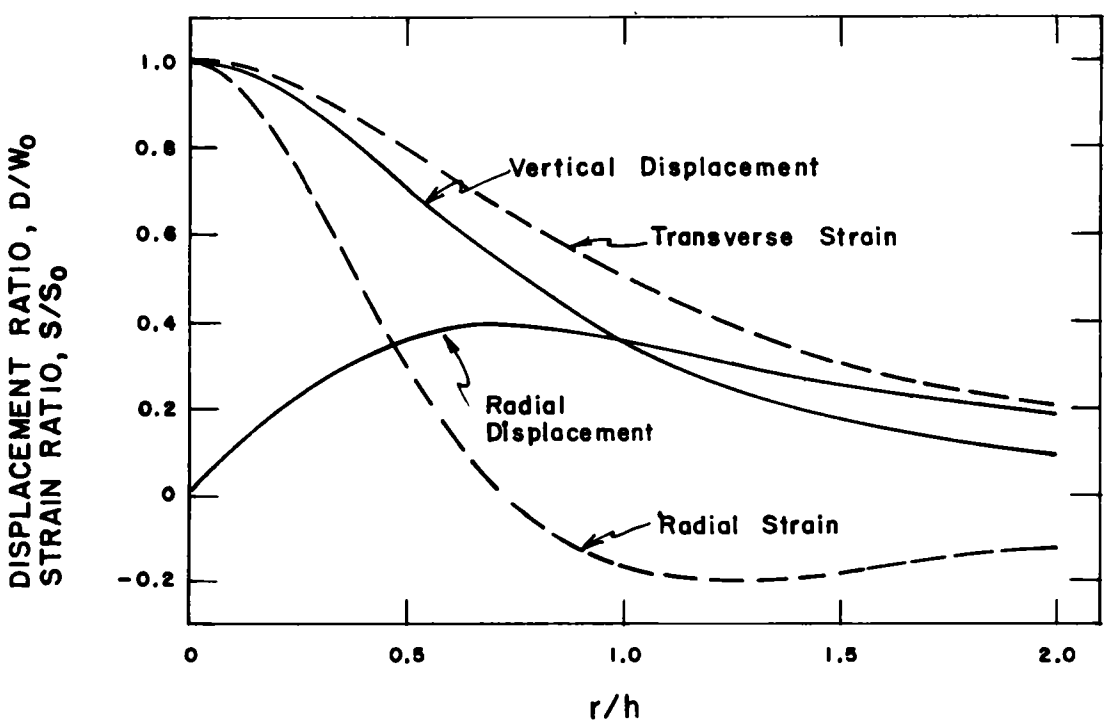

Fig. 2.3 Displacement and strain due to a buried pressure center in a semi-infinite elastic medium (r = ground range, i.e., distance from ground zero; h = depth of burial).

CHAPTER 3

INSTRUMENTATION

All 34 channels of instrumentation were essentially the same as those used on a number of previous projects (Reference 8).

3.1 RECORDING SYSTEM

In general, the instrumentation consisted of Wiancko 3-kc oscillators supplying carrier power to end instruments (Wiancko variable-reluctance accelerometers) and to Wiancko demodulators. The demodulated signal was applied to and recorded on Miller Corporation oscillograph recorders. Each channel was dual-recorded to minimize loss of data from failure of a single recorder. On some of the dual channels, galvanometers having different sensitivities were used to provide a wide dynamic range of usable sensitivities.

A synthetic "calibrating signal" was automatically applied to each recording channel just prior to zero time. This signal was used to compare record deflections with those obtained by the same signal or "cal tap" at the time the channel was calibrated.

A highly accurate timing signal of 100 and 1000 cps was also applied to all recorders simultaneously from a single source having a time accuracy of better than 10 parts per million. This gives the same time base to all records for time correlation of the separate events on all records.

All instrument recording gear was mounted in the SRI recording truck located on the mesa at approximately 2200 ft from ground zero (Fig. 3.1).

To prevent radiation damage to photographic records if Rainier shot were not contained, the oscillographs in the recording truck were protected by appropriate shielding. The truck body, camera cases, and paper magazines would afford a certain amount of shielding, about 0.5 cm of steel, 1.0 cm of aluminum, 5 ft of air and 2 cm of paper. Thus, the inherent shielding in the truck would have an attenuation factor of about 0.5 for 0.35-Mev gamma radiation.

If the radiation were as much as 15 r infinite this shielding would reduce the level to 7.5 r and recovery at H + 5 hours (200 mr/hr) would cut this amount to 5.2 r, giving a safety factor of over 2. To increase the safety factor still more, the oscillographs were shielded with lead bricks and lead sheets. This was done by stacking 1-1/2-inch thick lead bricks at the rear of the oscillographs opposite the paper magazines and placing 1/2-inch thick lead sheets under the oscillographs and on a framework which covered the tops and the fronts of the oscillographs. This covering gave a safety factor of 30 or more.

3.2 END INSTRUMENTS

3.2.1 Accelerometers. Standard Wiancko variable-reluctance accelerometers were used (Reference 9).

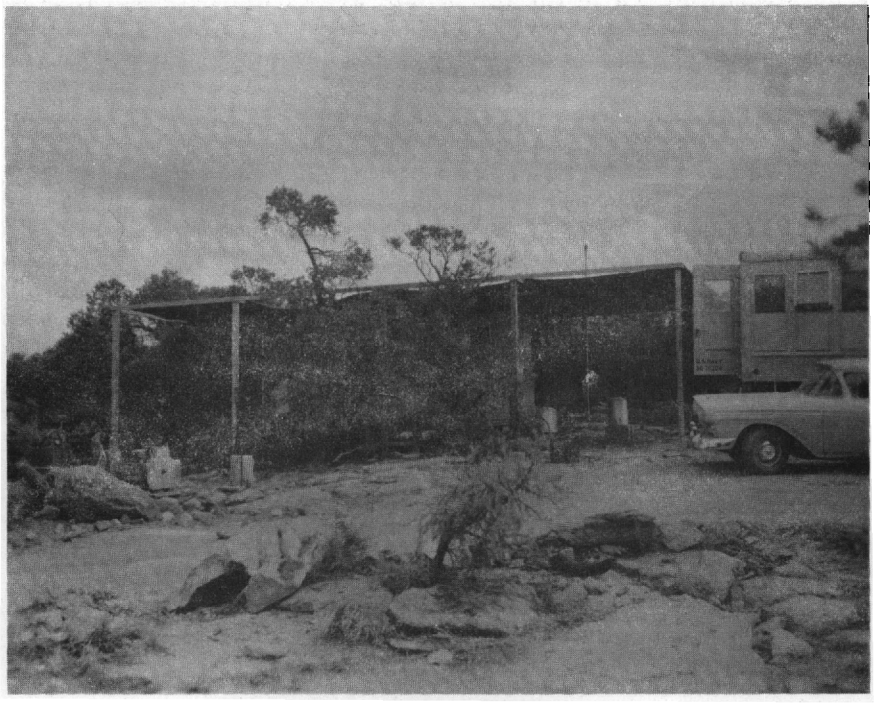

Fig. 3.1 Recording station on the mesa surface
(Recording truck under canopy)

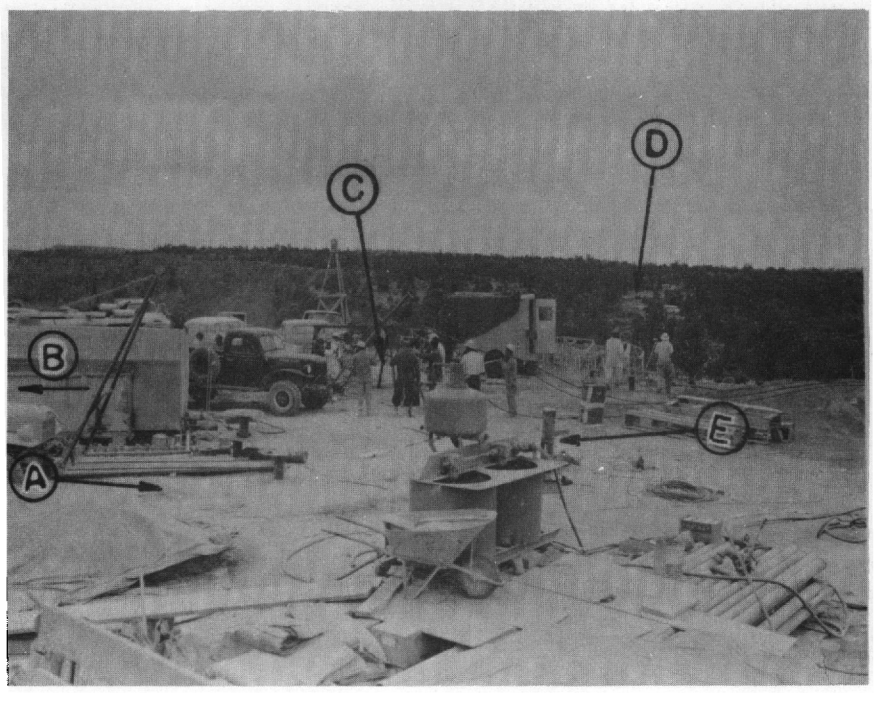

Fig. 3.2 Mesa surface; Ground zero and vicinity, looking south.
A - SRI, station 0, deep hole (accelerometers); B - Mesa edge; C - Sandia installation; D - SRI surface gage line; E - Ground zero (behind pipe).

The accelerometers in the deep hole at Station O (Fig. 3.2) were installed in the following manner: A 1/4-inch wire cable, which had been prestretched, was weighted and lowered into the hole. At measured points on the cable, the appropriate accelerometer for that depth was attached, together with its signal cable. At three points, as the entire array was being lowered into the hole, one-inch plastic hoses were also attached to the cable. After the accelerometers were stopped at the designated depths, a special grout, specified by Waterways Experiment Station, was pumped down these hoses until the hole was filled. Those on the mesa surface were encased in canisters which carried two accelerometers mutually perpendicular to each other so that both vertical and horizontal accelerations could be measured. The canisters were grouted in holes drilled or dug in the rhyolite cap (Fig. 3.3).

Accelerometers on the slope were mounted in perpendicular and radial positions by fastening them to wooden blocks which in turn were attached to the tuff by two bolts grouted into drilled holes (Fig. 3.4).

Accelerometers in the deep hole at ground zero were calibrated by use of a spin table with accelerations up to approximately 10 g. Accelerometers on the mesa and on the slope were calibrated in the earth's field by use of a turn-over cradle which gave equivalent accelerations to 2 g.

Accelerometers were calibrated in the field after they had been connected to their cables and associated recording equipment just prior to being grouted into the rock.

3.2.2 Strain Gages. The earth strain gages used on this project were an adaptation of the Ballistics Research Laboratory long-span displacement gages. They consisted essentially of a potentiometer whose shaft is arranged so that it can be rotated by a sheave wheel on the end of the shaft. A long length of piano wire was anchored at a distant point and was also attached to the sheave wheel. This wire was kept under tension by a coil spring so that any change in the relative position of the gage to the distant anchor results in a rotation of the potentiometer shaft thus indicating the change in the relative position of the two measured points.

Strain gages on the mesa surface and slope were mounted on a plywood board which in turn was anchored to the solid rhyolite by four bolts, which were also grouted into drilled holes (Fig. 3.5). The eye bolts for attaching the wire at the other end were also grouted to the rhyolite.

The strain gages were calibrated with 1- to 4-inch displacement blocks at the end of the wire span away from the gage and the appropriate deflection noted.

3.3 INSTRUMENT RESPONSE

The Wiancko accelerometer and its associated recording system is basically flat down to steady-state conditions due to its design as a carrier-demodulator system. No correction therefore is required for its low frequency response. The high frequency response is limited either by the characteristics of the galvanometers or by the dynamic characteristics of the

Fig. 3.3 Accelerometer installed on surface of mesa

Fig. 3.4 Accelerometer installed on slope of mesa

transducers. The 300-cps galvanometers (nominal) had a natural frequency of 315 to 340 cps and were damped to have an overshoot of approx. 7-1/2 percent. This corresponds to a damping factor of approximately 0.65 critical and provides a nominal rise time of 1.3 milliseconds. The 200-cps galvanometers were also critically damped and had a correspondingly longer rise time of approximately 1.8 milliseconds.

The accelerometers varied in sensitivity from 1 g to 10 g and in general had low natural frequencies so that the limiting frequency response was generally that of the accelerometers.

3.4 TIMING SIGNALS

Instruments were energized by Edgerton, Germeshausen, and Grier (EG&G) timing signals that actuated lock-in relays controlled by a time-delay relay which allowed continued instrument operation for approximately two minutes after zero time, even though EG&G relays dropped out sooner.

3.5 POWER SUPPLY

During the shot, all instruments and recorders were supplied with power by banks of heavy duty batteries. Converters were used to produce 115-volt a-c for instruments requiring this power. Individual converters were used for each rectifier power supply to minimize possible gross failure due to converter failure. During calibration and testing before the shot, a 10-kw motor generator was used as a power source.

3.6 GAGE CODING

For identification of channels and recorded traces with their proper gages, a systematic coding was used. The first part of the gage code is the station number. Letters which indicate the type of measurement form the second part of the gage code. On this project the letters AP denote vertical or perpendicular acceleration; that is, vertical or perpendicular with reference to the natural terrain. The gages on the mesa surface and in the hole would be vertical while those on the slope would be perpendicular to the tuff out-crops but not necessarily perpendicular to the horizontal plane. AH denotes horizontal radial acceration, ST denotes transverse strain, and SH denotes horizontal radial strain. The third part of the gage code, applicable only at Station 0 indicates the depth of the gage below the surface in feet. Typical gage code numbers would then be as follows: 3AP for Station 3, vertical acceleration; 0AP180 for Station 0, vertical acceleration at a depth of 180 ft.

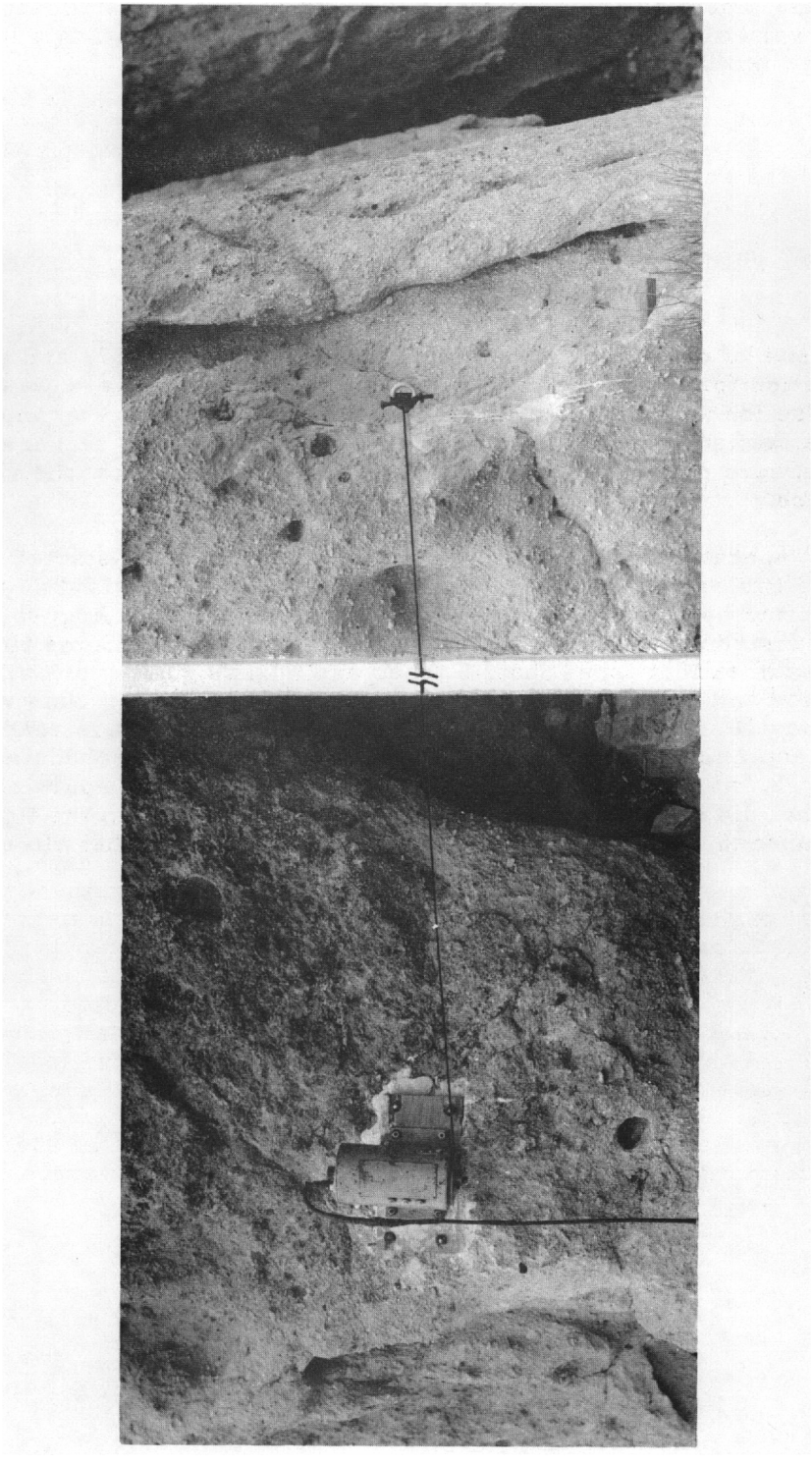

Fig. 3.5 Typical strain gage installation (spans varied).

CHAPTER 4

OPERATIONS

The site of operations was examined on April 26, 1957, and at that time a location for the recording truck was chosen. The mesa was scouted, and the direction and approximate location of the line of accelerometer and strain gage stations was also chosen. The mesa slope was traversed, and four places were picked for installation of stations just below the rhyolite-tuff interface.

Field operations in preparation for this project were started on August 13. All the cables to surface stations on this project were laid on the ground only, protected by culverts where they crossed roads. By August 21 cables were laid, instruments connected, and calibration begun. Some time was lost because of fallout from Shots Galileo and Fizeau; however, all gages were in place and calibrated by September 17. Final timing runs were made on September 18, and the instruments were checked and made ready in the evening of September 18. The shot, which was originally scheduled for September 18, was delayed 24 hours and detonated at 1000 hours on September 19. The shot did not vent and after a few hours, the road to the top of the mesa was opened, and recovery of the records was made that afternoon.

CHAPTER 5

RESULTS

5.1 PERFORMANCE

All 34 instrument channels installed gave usable records, although 4 were incomplete due to cable breaks during the active portion of the record. The breaks occurred in the cables associated with the underground accelerometers; however, enough of the gage records was obtained to lead to definitive conclusions.

Because some of the predicted values for peak acceleration proved to be low, some of the gage records exceeded the boundaries of the recording paper. Nevertheless, since each gage record was recorded twice, often with galvanometers of different sensitivities, it was possible in almost all cases to determine the magnitudes of the peak accelerations at each station.

All accelerometers and strain gages on the mesa top were recovered and appeared to suffer no permanent damage. On the slope, the Station 10 gages were lost due to a rock slide in that vicinity; one accelerometer was missing at Station 11, also probably the victim of falling rock; the gages at Stations 12 and 13 were recovered intact.

5.2 DATA REDUCTION

After identification of the gage records on each oscillogram, the arrival times, peak deflection, and times of peak deflection were read from the original records. All readings were taken manually with simple scales, and computations were made with a slide rule. Since there were a number of crossover traces creating possible confusion, it was desirable to trace the records to separate them for examination of wave form characteristics and for further treatment. Records of vertical (perpendicular) acceleration were integrated with a planimeter to obtain particle velocity and displacement versus time.

It should be emphasized that the data presented in this report are preliminary and may be changed materially when subjected to careful data reduction procedures.

5.3 RESULTS

Tracings of the individual gage records are shown in Figs. 5.1 through 5.7. These records represent the raw data and have not been edited in any way. No attempt has been made to normalize the records to a common time or acceleration scale. Included on these figures are the times of arrival and the designation of peak values of acceleration or strain.

5.3.1 Earth Acceleration.

Figures 5.1 through 5.5 present the tracings of the earth acceleration records. The vertical acceleration versus time curves (Figs. 5.1 through 5.3)

are mostly characterized by a single peak of acceleration in the positive direction (away from the detonation point) followed by a negative acceleration and a second definite positive peak. Figure 5.1 shows the results of the underground acceleration measurements taken in the deep hole; this figure includes all of the records that were influenced significantly by cable breakage. The vertical accelerations measured on the mesa line are presented in Fig. 5.2, while Fig. 5.3 shows the results obtained on the slope. The horizontal acceleration records for the mesa and slope lines are included in Figs. 5.4 and 5.5, respectively.

The basic acceleration data are presented in Table 5.1 and 5.2. The results of rough integration of the acceleration-time records to obtain earth particle velocity and displacement are listed in Table 5.3. The tabular data are all as-read and must be considered as preliminary. Whenever dual channels were employed on a single gage, an average value of the two results is shown in the table.

5.3.2 Earth Strain.

Figures 5.6 and 5.7 present the tracings of the earth strain records. It is seen that most of the records are characterized by low amplitudes and long rise times. Table 5.4 includes the basic strain data. The residual strain shown on Figs. 5.6 and 5.7 is read on the record after the trace has apparently settled down to a steady value.

TABLE 5.1 EARTH ACCELERATION, PERPENDICULAR COMPONENT, SHOT RAINIER

Station No. and Gage code	Nominal ground range, ft	Gage depth, ft	Radial distance, ft	Arrival time, sec	First peak* accel., g	Time of first peak, sec	Max. † pos. accel., g	Time of max. pos., sec	Max. neg. accel., g	Time of max. neg., sec	Remarks
0AP320	0	320	582	0.089	5.73	0.106			0.77	0.187	Cable break at 0.205 sec.
0AP250	0	250	652	0.101	1.35	0.119			0.75	0.282	Cable break at 0.325 sec.
0AP180	0	180	721	0.110	0.92	0.130			0.38	0.325	Cable break at 0.325 sec.
0AP100	0	100	800	0.123	3.90	0.150			1.0	0.350	Cable break at 0.470 sec.
0AP	0	0	900	0.146	5.83	0.186			1.1	0.280	
1AP	450	0	968	0.158	3.09	0.186	5.10	0.406	1.50	0.454	
2AP	650	0	1095	0.179	3.04	0.209	>6.3	0.430	1.04	0.327	Trace off record at 0.430 sec.
3AP	900	0	1269	0.202	1.50	0.226			0.96	0.316	
4AP	1250	0	1541	0.245	0.90	0.281	2.04	0.467	0.76	0.361	
5AP	1900	0	2017	0.296	0.56	0.356	0.78	0.538	0.62	0.465	
6AP	2500	0	2518	0.357	0.37	0.420	0.44	0.603	0.46	0.462	
10AP	0	0	798	0.146	7.93	0.171			3.06	0.203	
11AP	400	0	860	0.146	8.50	0.169	9.49	0.636	>3.25	0.490	Trace off record at 0.490 sec.
12AP	800	0	1083	0.173	1.59	0.215	2.02	0.408	0.95	0.294	
13AP	1500	0	1771	0.275	0.40	0.325	0.43	0.493	0.83	0.361	

* Positive acceleration is away from detonation point; negative acceleration is toward detonation point.

† Maximum positive acceleration is listed only if different from first peak acceleration.

TABLE 5.2 EARTH ACCELERATION, HORIZONTAL COMPONENT, SHOT RAINIER

Station No. and Gage code	Nominal ground range, ft	Radial distance, ft	Arrival time, sec	First peak* accel., g	Time of first peak, sec	Max. † pos. accel., g	Time of max. pos., sec	Max. neg. accel., g	Time of max. neg., sec	Remarks
1AH	450	968	0.159	1.08	0.188	2.22	0.417	4.2	0.407	Maximum negative peak estimated
2AH	650	1095	0.176	0.92	0.204	>6.6	0.430	3.1	0.435	Trace off record at 0.430 sec.
3AH	900	1269	0.200	0.61	0.229	0.66	0.698	0.80	0.476	
4AH	1250	1541	0.248	0.55	0.306			0.55	0.540	
5AH	1900	2017	0.297	0.41	0.358	0.73	0.765	0.44	0.585	
6AH	2500	2518	0.365	0.33	0.426	0.46	0.862	0.33	0.516	
11AH	400	860	0.145	3.24	0.169	8.55	0.635	>3.1	0.495	Trace off record at 0.495 sec.
12AH	800	1083	0.175	1.37	0.215			>1.47	0.450	Trace off record at 0.450 sec.
13AH	1500	1771	0.276	0.66	0.328	1.07	0.532	0.50	0.556	

* Positive acceleration is away from ground zero; negative acceleration is toward ground zero.

† Maximum positive acceleration is listed only if different from first peak acceleration.

TABLE 5.3 EARTH STRAIN, HORIZONTAL AND TRANSVERSE COMPONENTS, SHOT RAINIER

Station No. and Gage code	Nominal ground range, ft	Radial distance, ft	First peak* strain, ppk	Time of first peak, sec	Max. pos. † strain, ppk	Time of max. pos., sec	Max. neg. † strain, ppk	Time of max. neg., sec	Residual strain, ppk
0SH	0	900	+ 3.34	0.577			0.694	0.850	+ 1.50
2SH	650	1095	- 0.261	0.23-0.43	0.506	1.180			+ 0.41
3SH	900	1269	- 0.084	0.4 -0.7	0.227	1.40			+ 0.112
4SH	1250	1541	- 0.039	0.32-0.38	0.080	1.0			0
5SH	1900	2017	- 0.10	0.54-0.69	None				- 0.023
10SH	0	798	+ 0.239	0.240	3.13	0.800	1.36	0.485	Cable break (or wire break)
11SH	400	860	+ 0.37	0.22-0.26			5.21	0.630	- 2.57
0ST	0	900	- 0.50	0.195	4.35	0.610			+ 1.61
2ST	650	1095	+ 0.116	0.430	0.282	0.620	0.293	0.960	- 1.75
3ST	900	1269	+ 0.63	0.590			0.061	0.900	+ 0.26

* Positive strain is increase of wire span length; negative strain is decrease of wire span length.

† Maximum positive strain (or maximum negative strain) is listed only if different from first peak strain.

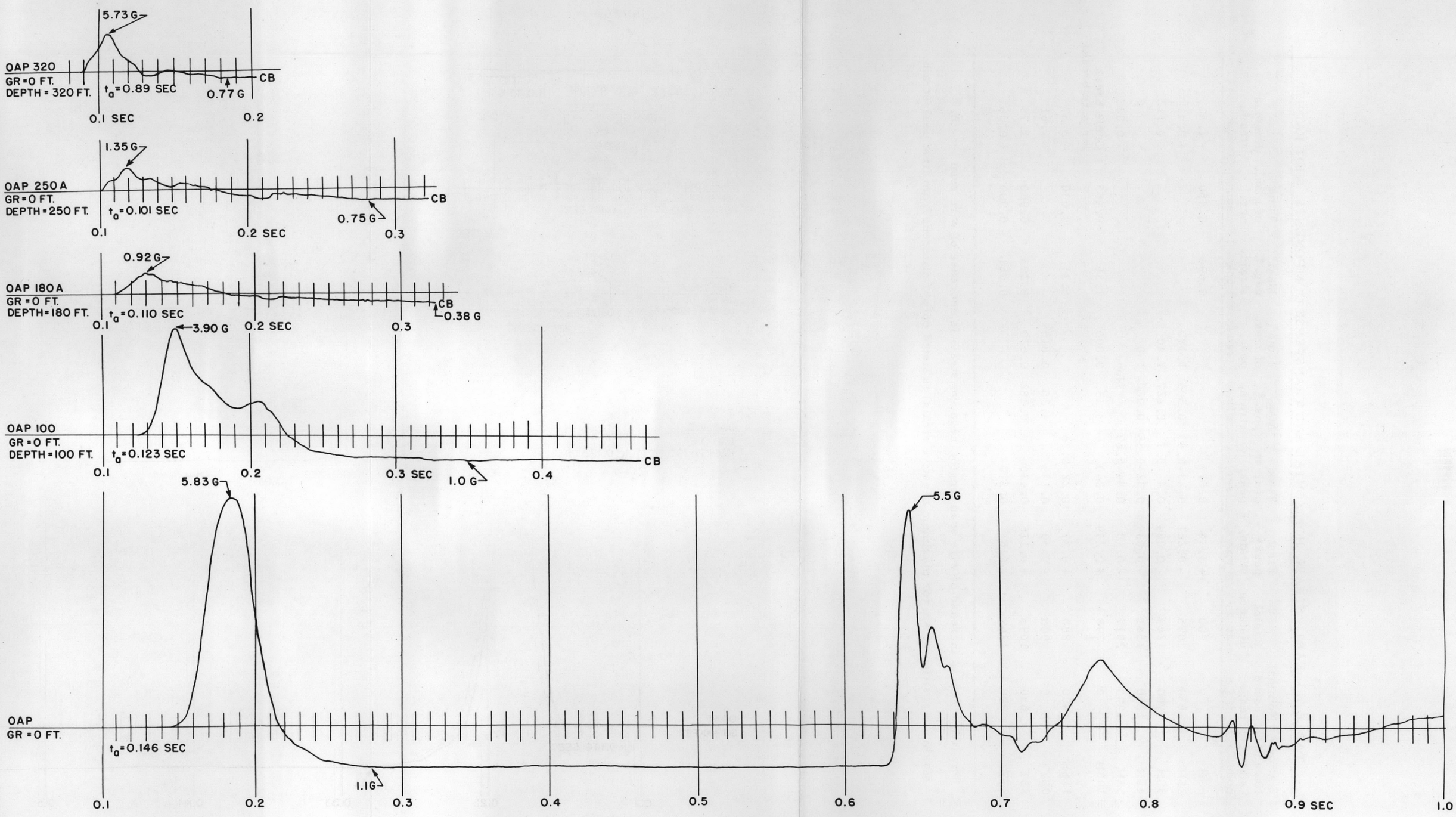

Fig. 5.1 Vertical acceleration records, deep hole, shot Rainier

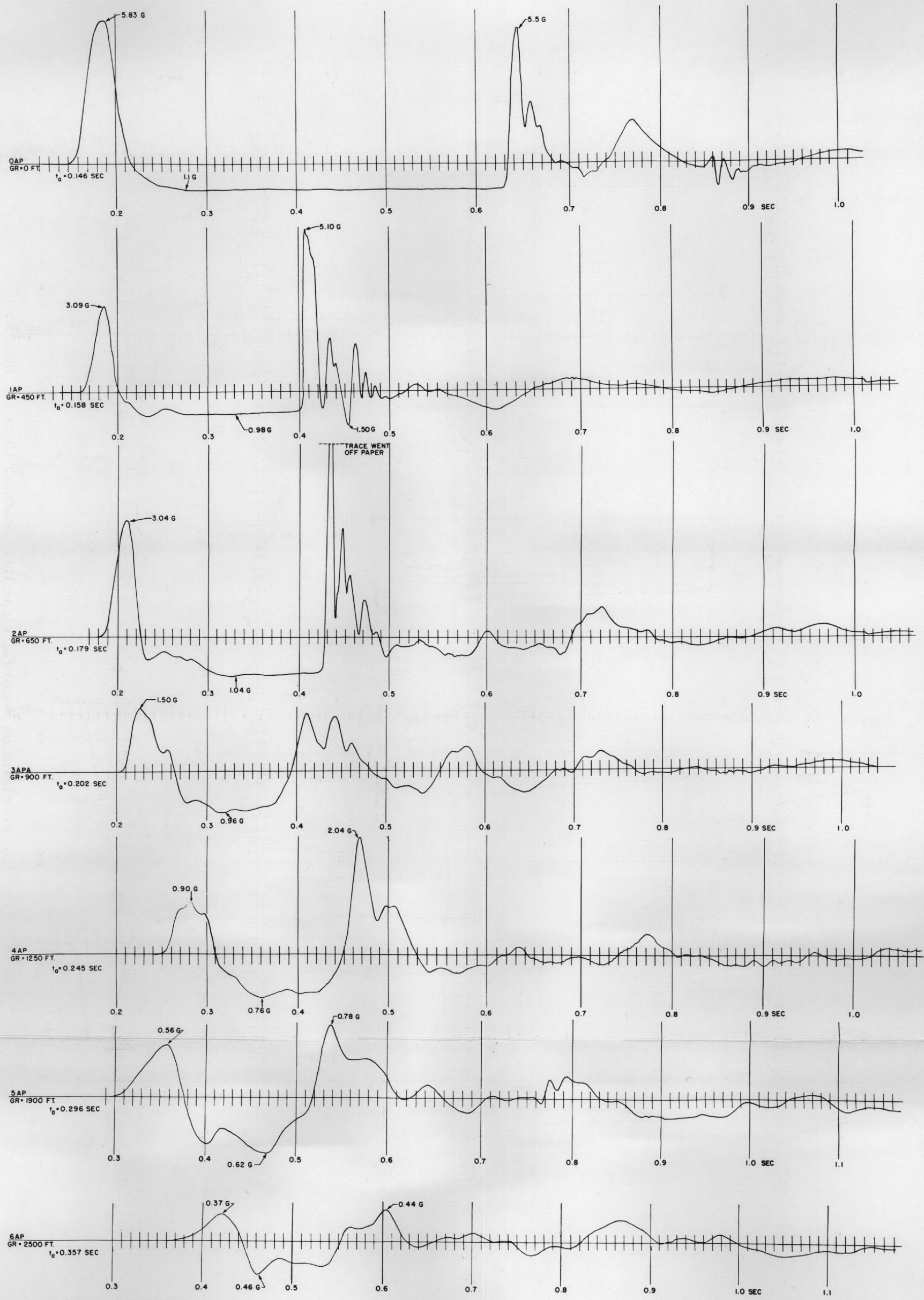

Fig. 5.2 Vertical acceleration records, mesa line, Stations 0 to 6, Shot Rainier

Fig. 5.3 Vertical acceleration records, slope line, Stations 10 to 13, Shot Rainier

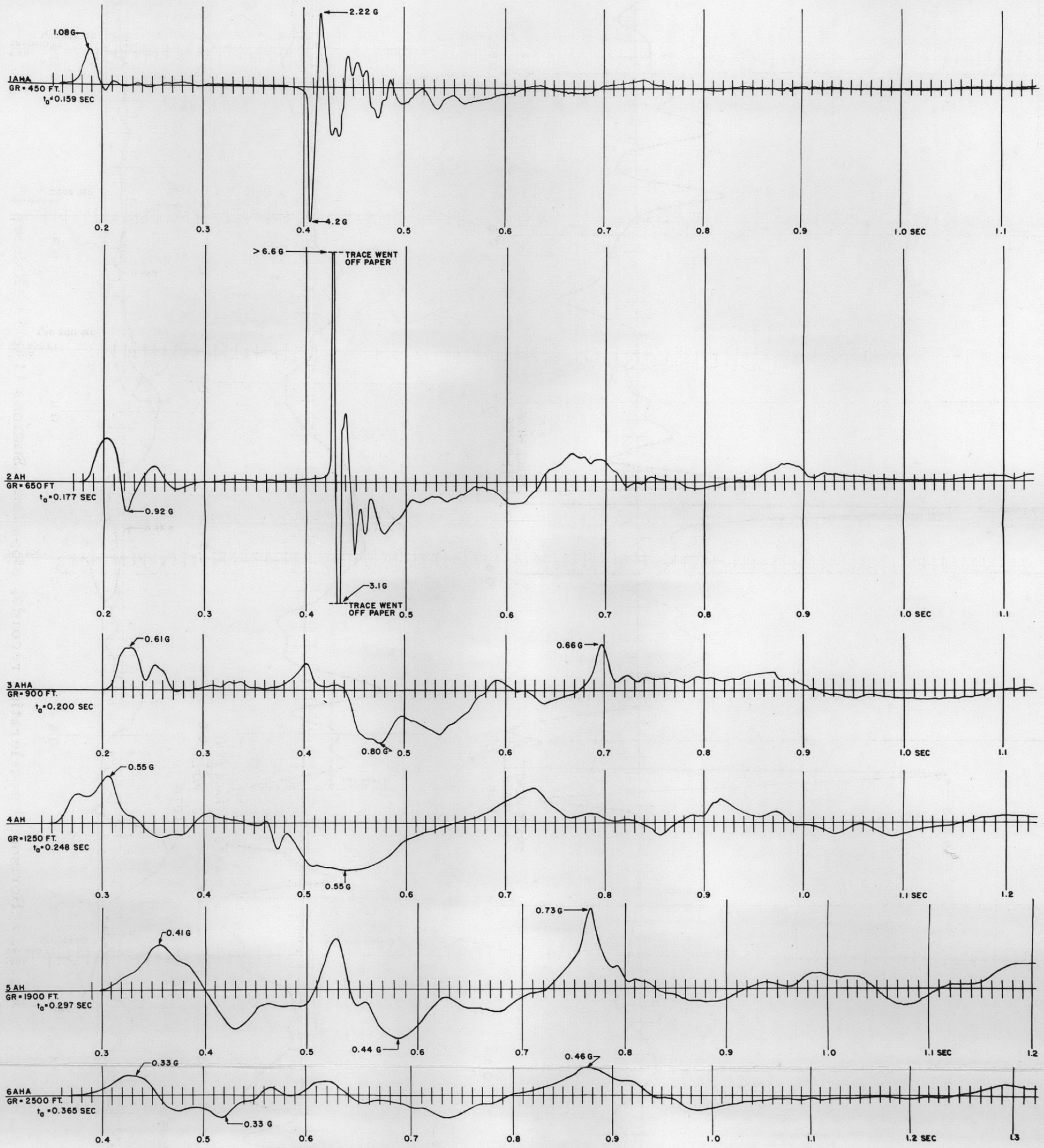

Fig. 5.4 Horizontal acceleration records, mesa line, Stations 1 to 6, Shot Rainier

Fig. 5.5 Horizontal acceleration records, slope line, Stations 11 to 13, Rainier

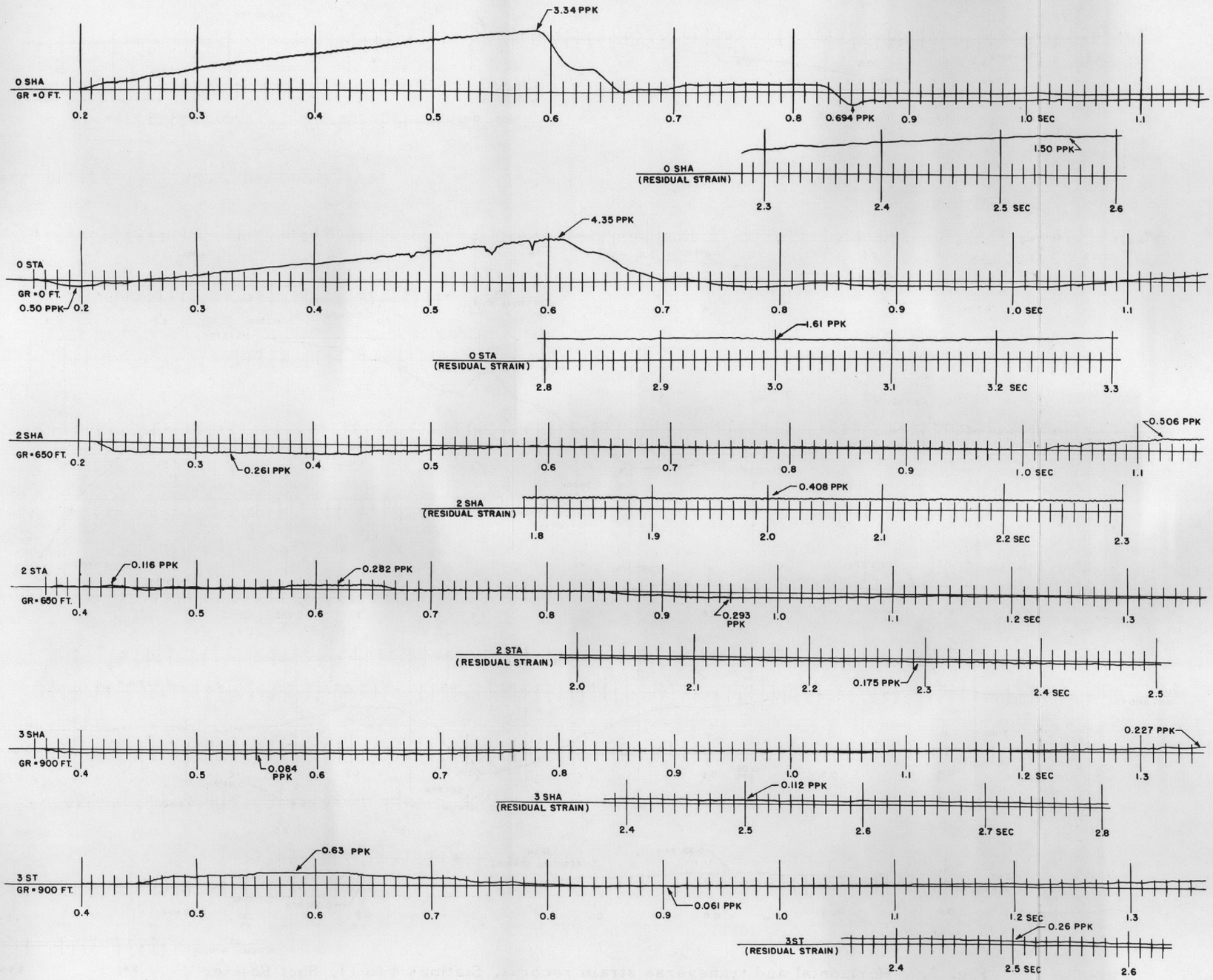

Fig. 5.6 Horizontal and transverse strain records, Stations 0 to 3, Shot Rainier

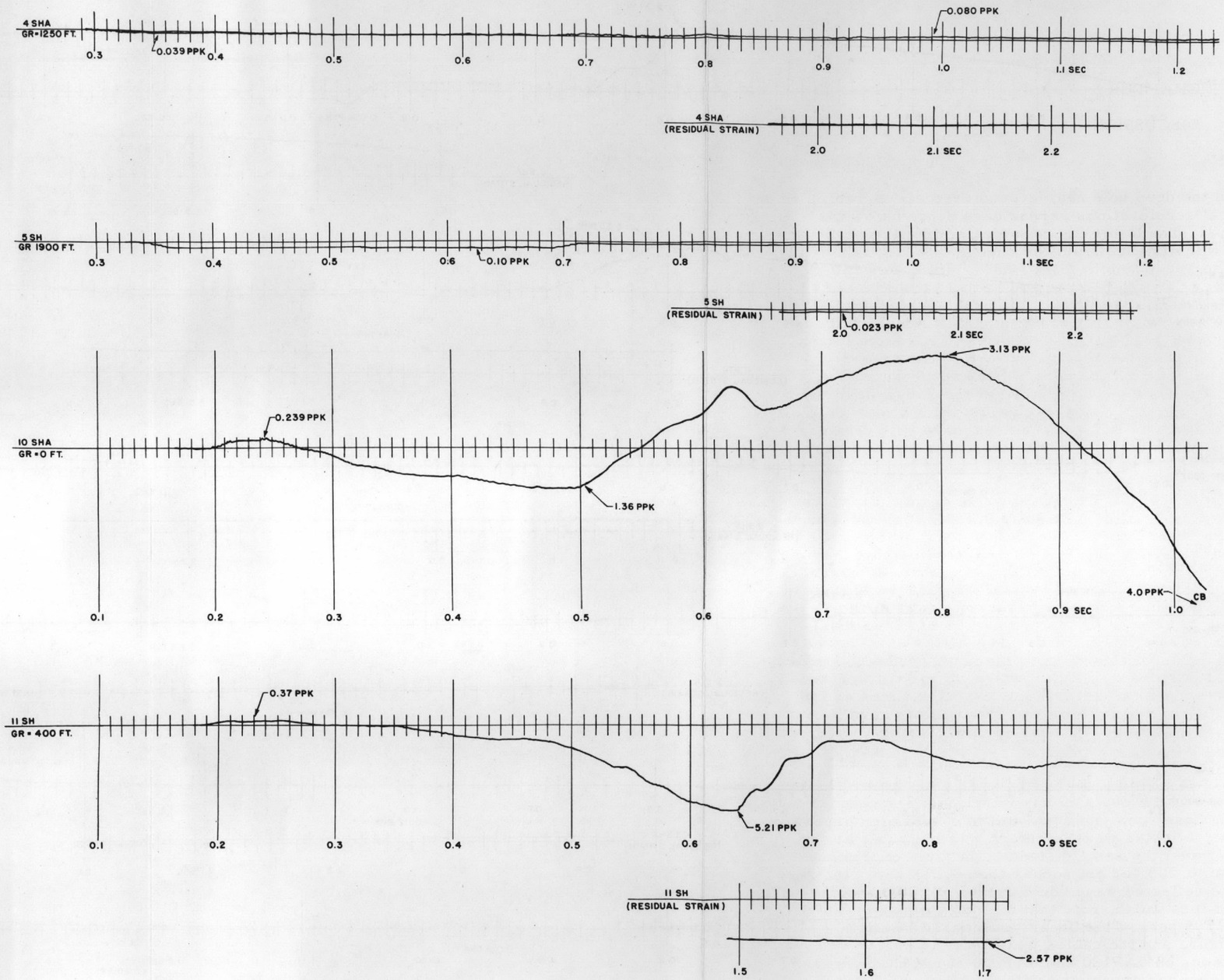

Fig. 5.7 Horizontal and transverse strain records, Stations 4 to 11, Shot Rainier

CHAPTER 6

DISCUSSION

6.1 EARTH ACCELERATION

The records obtained in the deep hole near ground zero are shown in Fig. 5.1, and the peak vertical accelerations versus gage depth below the surface are plotted in Fig. 6.1. The latter figure indicates that the peak vertical acceleration decays with distance from the charge in a regular fashion from 320-ft to 250-ft to 180-ft depths (i.e., 580-, 650-, and 720-ft distance from charge); however, at 100-ft depth and at the surface there is a decided deviation from this regular behavior, the peak acceleration at the surface registering more than 5 time that observed 180 ft deep. Although cable breaks do not allow complete verification of the deep gage wave forms, the wave forms appear to be following the general pattern of the record obtained at the surface (0AP) before the cables were broken. Figure 6.1 indicates that although the acceleration peak recorded at the 320-ft depth was close to preshot prediction, the other measurements deviate markedly from estimates. The observed severe decay of peak response with distance from the explosion and the abrupt increase at 100 ft and at the surface were contrary to prediction.

Figure 5.1 reveals some additional interesting phenomena. First, it is believed that the secondary acceleration peak (near 0.2 sec) observed on the 0AP100 record is due to the stress wave reflected (in tension) from the ground surface. As explained in Section 2.2.3, this reflected tension (negative stress) wave will produce a positive (upward) acceleration. Whereas the incident compression wave and the reflected tension wave at the surface coincide in time and produce together a single acceleration peak, at the 100-ft depth the tension wave peak should lag the compression stress maximum by the length of time it takes a stress wave to travel to the surface and return. The 0AP100 record is consistent with this explanation; the secondary acceleration pulse occurs at the expected time. Further, it may be concluded that, since no second acceleration peak is observed at expected times on the 0AP180 or 0AP250 records, the earth must have fractured somewhere below the 100-ft depth; moreover, the wave was destroyed by the fracture since no further reflections are evident.

Assuming that the earth, as a jointed medium, could not support tension, the fracture must have occurred at the depth at which the tensile stress (in the wave reflected from the surface) was just equal to the overburden pressure. Assuming that the time for the reflected wave to return was the same as the time for the primary wave to travel the same distance, the time of fracture can be fixed as being later than 0.205 sec but sooner than 0.218 sec, that is, between the times at which the reflected wave could arrive at 100-ft depth and at 180-ft depth. For what it is worth, note that the cable break on the 0AP320 record occurred at 0.205 sec. This break was caused by earth movement somewhere in the hole, and the cables were indeed grouted into the hole. The small disturbances on 0AP180 and 0AP250 at the same time were no doubt electrical disturbances associated with the first cable break.

If the above explanation of fracture is correct, an additional observation is pertinent. As the yield of the device increases, the stress wave would be

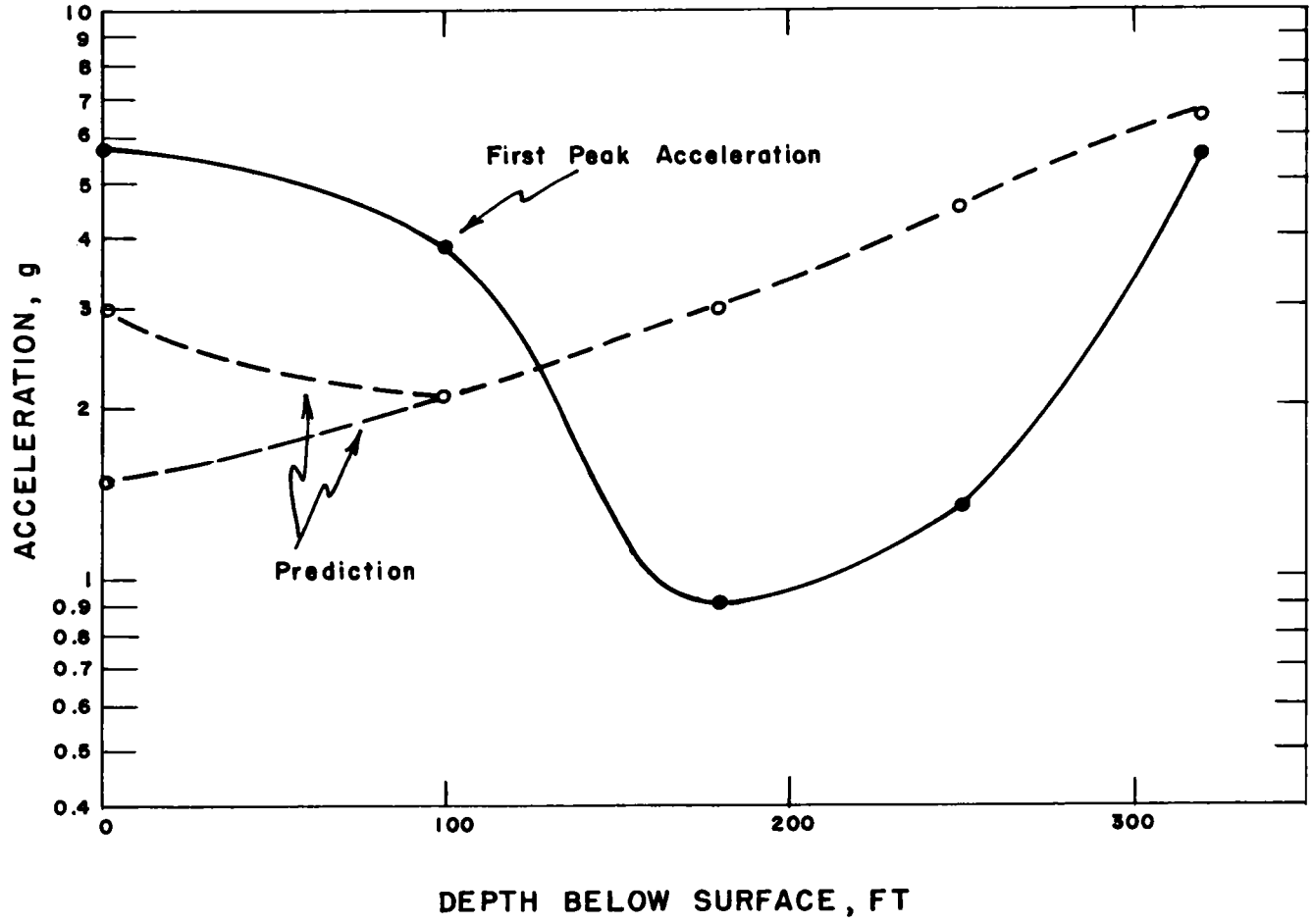

Fig. 6.1 Maximum vertical acceleration vs depth in deep hole

longer in time and space, therefore, the reflected tensile stress wave would build up to significant magnitude at greater and greater depths. Futhermore, since the overburden pressure to be overcome for fracture also increases with depth, one can be optimistic (rather than pessimistic) about the possibility of containing a larger yield device at the same scaled depth as Rainier.

From the vertical acceleration measurements made on the surface (Fig. 5.2), the following facts become evident:

1. The gage records, particularly out to 650-ft range, are of the same general appearance, i.e., an initial positive (upward) acceleration peak followed by a long negative phase and then another positive peak.

2. The initial acceleration pulse is identified with the motion of the overburden due to the detonation energy arriving at the ground surface. It will be noted that the negative phase amplitude in most cases (0AP, 1AP, 2AP, and 3AP) is approx. 1g; this suggests that the earth surface at these radii was thrown up and was subsequently in free fall for several tenths of a second. There is evidence that there was a separation of the earth medium at some depth, a fact which will be verified when particle velocity and displacement are discussed (Section 6.2).

3. The second acceleration pulse is interpreted as the bottoming of the surface section as it fell back onto the main mass of the mesa. The shock pulse must have been initiated at the contact interface at depth and then transmitted to the surface.

4. The region around Station 1 bottomed considerably before that around Station 0 and slightly before that at Station 2 (Fig. 5.2). This time interval between Stations 0 and 1 is so great that there must have been a serious fracture between these gage stations so that two separate pieces of material fell back. This conclusion is substantiated by the 11APA record (Fig. 5.3) which shows evidence of two distinct bottomings of approximate equal intensity.

The multiple peaks associated with the second main acceleration pulse (Figs. 5.2 and 5.3) are probably due to reflections of the second pulse near the surface. The fact that the reflections appear so regular at some of the stations (especially Station 1AP) makes attractive a harmonic analysis of the less regular records at some of the other stations; this analysis will be deferred until the final report.

The acceleration records at many stations seem to show a sharper (and larger) shock when the blocks of rock bottomed than when they were thrown up. This can be explained by the fact that the block probably moved up with the moving substrate before separation occurred; however, when the block returned and bottomed, the substrate had fallen somewhat and was more nearly stationary. Thus, the time of stopping would have been much shorter than the time of starting; i.e., if the two impulses were equal, the bottoming force (or acceleration) would be the larger.

The maximum vertical acceleration (first peak) is plotted as a function of ground range (or radial distance) in Fig. 6.2. The figure indicates that

for the two stations closest to ground zero on the slope (Stations 10 and 11) the maximum vertical accelerations were significantly larger than those measured on the mesa top. Also included on the figure is the preshot prediction curve for peak acceleration taken from values of Fig. 2.3. It is evident from this figure that only at ranges larger than about 1000 ft from the detonation do the measurements approximate the predictions. Of course, the predictions did not include the possibility that the disturbance would take the form of a separation along a nearly horizontal bedding plane within the rhyolite cap.

Figures 5.4 and 5.5 indicate that the conclusions cited with regard to the vertical measurements are reinforced by the horizontal results. The horizontal acceleration records at Stations 1 and 2 (1AHA and 2AH) show virtually zero radial acceleration of the earth cap during the period between initial peak and bottoming response, which confirms the idea of free fall; also, the time of free fall indicated on these records is consistent with the vertical records (Fig. 5.2). At both stations, the initial upward acceleration pulse contained a radial component directed away from ground zero; also, the horizontal records indicate that the earth cap containing Stations 1 and 2 bottomed before the cap containing Station 0.

The horizontal accelerations produced by the elastic wave which travelled from the plane of impact to the surface show several fluctuations between positive and negative accelerations, which were produced by multiple reflections from planes at shallow depths. These reflections do not agree in form and in arrival times with the reflections recorded at the same stations on the vertical accelerometers. It is possible that the (really minor) disagreements in arrival times and sign of the reflected waves which were recorded between 0.4 and 0.5 sec on 1AH, 1AP, and 2AH, 2AP, are due to the fact that 1AH and 2AH were recording shear waves, while 1AP and 2AP were recording longitudinal waves. An explanation based on this possibility would go on to say that shear waves travel more slowly than longitudinal waves, so that even if they were reflected from the same depth, they would arrive later, However, since the reflection of the longitudinal waves from two or three depths would produce a pattern of arrivals of these reflections which is not simple, this explanation is discarded. Furthermore, the arrival of a longitudinal plane wave at Station 1 or 2 could produce horizontal as well as vertical accelerations, provided the plane of the wave is inclined to the horizontal.

Plane longitudinal waves reflected from various depths could easily arrive in planes inclined to the horizontal, and almost any combination of positive and negative horizontal accelerations can be arranged for by only moderate changes in the geometries of the reflecting surfaces. For example, the first pulse that arrived at 1AH from the "bottoming" was a radial acceleration towards ground zero, whereas as 2AH the first pulse was radially away from ground zero. This could be explained by the geometry of Sketch C at right; that is,

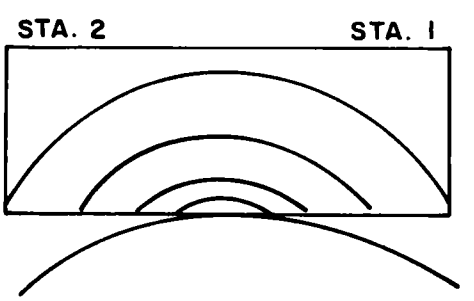

(In this model it is assumed that seismic rays were straight lines.)

Sketch C

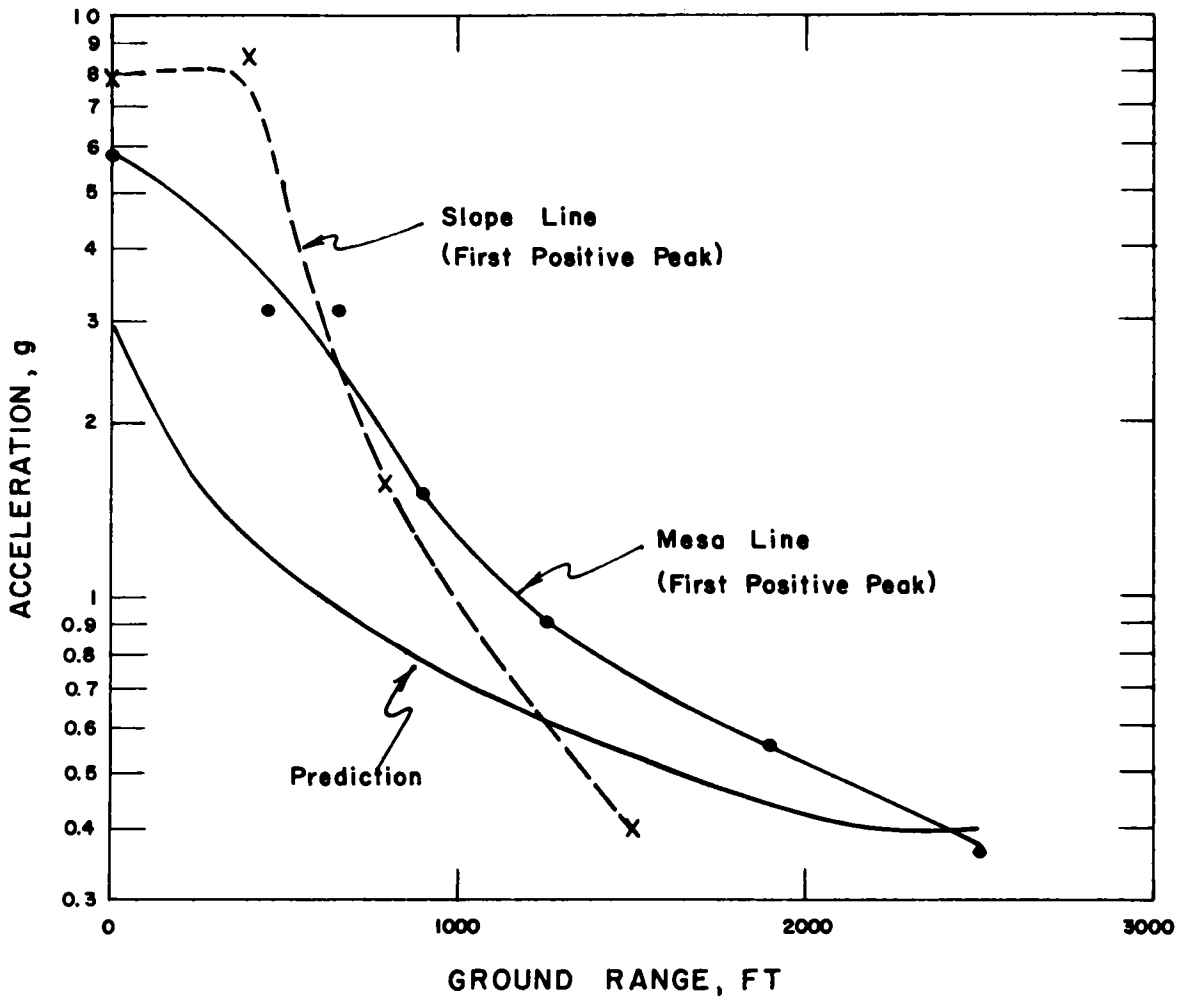

Fig. 6.2 Maximum vertical acceleration vs ground range (mesa and slope)

by the assumption that "bottoming" was really achieved at first only at the center of the bottom of the cap to which the gages were attached.

6.2 EARTH PARTICLE VELOCITY AND DISPLACEMENT

Crude integration of the acceleration-time records to obtain earth velocity and displacement yields some interesting results; Table 6.1 lists the significant data.

The results of the integration of the deep hole acceleration records are shown in Fig. 6.3. From the velocity-time curves, it is obvious that the earth parted at some depth between 100 and 180 ft; whereas at 180-ft depth the velocity is zero at about 0.3 sec, the velocity at a corresponding time 100 ft deep is about 3.0 fps positive (upward). This evidence supports the conclusion that a thick earth cap was thrown into the air. Although Fig. 6.3 indicates that the velocity at the surface was higher than that at 100-ft depth, it is unwise on the basis of the crude integration procedure to assign any significance to this result.

The displacement-time curves (Fig. 6.3) show a behavior similar to particle velocity. The displacement at 320-ft depth is not the maximum displacement; the gage cable broke (indicated by CB on Fig. 6.3) before zero velocity was attained. Here again, one should not assign any significance to the difference between displacement-time curves from the 100-ft deep and surface measurements; the apparent constant differential suggests that the linear calibration used for preliminary data reduction was probably inadequate for one of the measurements.

Using the displacement-time curves from all the mesa line stations, it is possible to construct the curves shown in Fig. 6.4, which represent the approximate vertical elevation contours (above preshot levels) at various times after detonation (the vertical scale has been greatly expanded to give readable curves). The contours indicate that the most significant surface displacement occurred near Station 0, with the contours falling off abruptly out to about 500 ft. Also, the crack or break which was mentioned in connection with the acceleration records is corroborated by the obvious difference in vertical displacement between Stations 1 and 2 at about 0.3 sec. However, close examination of the data shows that this difference in displacement is only about 0.75 inch; although this is much larger than can be ascribed to integration inaccuracies, it is so small that perhaps it was not observed by the shot photography. It is rather apparent that the chunk which contains Station 1 (450-ft ground range) would bottom before the piece containing Station 2 (Fig. 5.2).

Also shown on Fig. 6.4 is the normalized vertical displacement contour for the static case (see Appendix B). As one would expect, this static contour shows the displacement decaying with distance much more slowly than was observed on Rainier shot; it is possible that the post-shot survey of permanent displacement at the ground surface will reveal a contour which resembles the static one more closely.

TABLE 6.1 EARTH VERTICAL PARTICLE VELOCITY AND DISPLACEMENT, SHOT RAINIER

TABLE 6.1 EARTH VERTICAL PARTICLE VELOCITY AND DISPLACEMENT, SHOT RAINIER

Station No. and Gage code	Nominal ground range, ft	Radial distance, ft	Maximum velocity, fps	Time of max. vel., sec	Maximum displacement, ft	Time of max. displacement, sec	Remarks
0AP320	0	582	3.2	0.13	0.28	0.205	Cable break at 0.205 sec.
0AP250	0	582	3.2	0.13	0.28	0.205	Cable break at 0.205 sec.
0AP180	0	652	1.3	0.18	0.12	0.27	Cable break at 0.325 sec.
0AP140	0	721	1.0	0.18	0.12	0.30	Cable break at 0.325 sec.
0AP100	0	800	4.9	0.23	1.0	0.42	Cable break at 0.470 sec.
0AP	0	900	6.4	0.22	0.94	0.43	
0AP	450	968	1.5	0.20	0.11	0.29	
1AP	450	1095	2.3	0.22	0.19	0.33	
2AP	650	1269	0.82	0.26	0.055	0.33	
3AP	900	1541	0.72	0.31	0.048	0.37	
4AP	1250	2017	0.72	0.38	0.046	0.44	
5AP	1900	2518	0.43	0.44	0.023	0.49	
6AP	2500	2518	0.43	0.44	0.023	0.49	

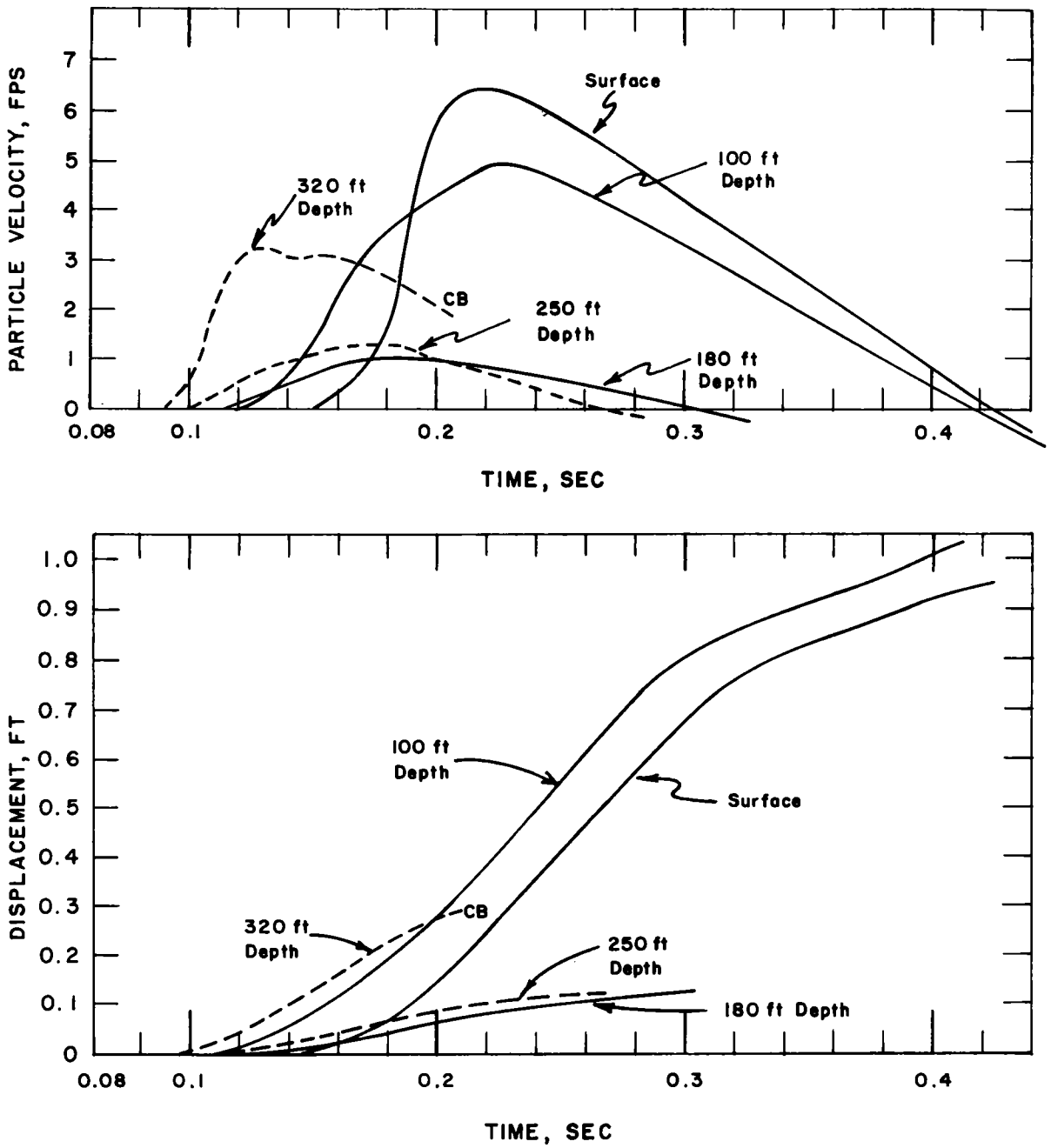

Fig. 6.3 Earth particle velocity and displacement vs time in deep hole

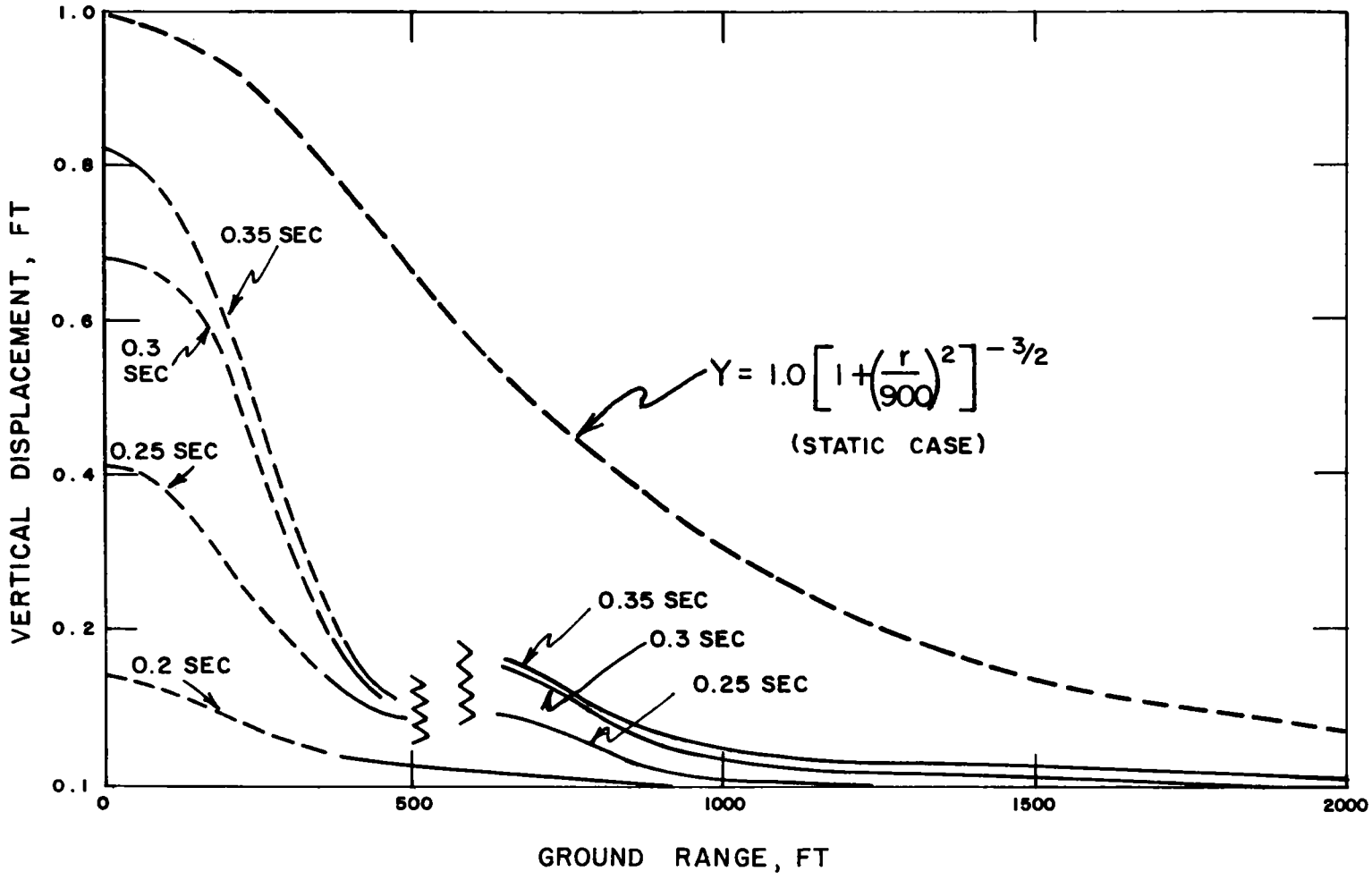

Fig. 6.4 Surface vertical displacement contours at various times

6.3 SEISMIC VELOCITIES

Velocities can be computed from data obtained from the nuclear shot, as well as from the subsidiary prior seismic survey made by U. S. Geological Survey (USGS).

The survey performed by USGS was conducted by exploding charges at the bottom of a 100-ft hole and recording arrivals at various depths in a survey hole 200 ft away, and at points on the surface between the holes. Both holes were vertical; the survey hole was 800 ft deep; the top 400 ft was cased, and geophones were hung in the hole (air coupling). Since horizontal distance between holes was but double that of the charge depth many of the seismic rays were horizontal, and most were slanted.

Anomalous velocities were obtained in this survey. Horizontally from shot point to survey hole, the velocity measured was 2600 fps; slant velocities from shot point to shallower points in the survey hole were in the range 2600-2900 fps. These velocities correspond to paths that deviate not more than 30° from horizontal.

The seismic rays travelled in more nearly vertical paths to those geophones which were on the surface, between the holes. The velocities measured were the greater, the more nearly vertical were the paths; the measured velocities increased from 2900 fps to 3800 fps. Unfortunately, no geophone was placed directly beside the shot hole. The survey therefore indicates fairly high differences between horizontal and vertical velocities in the rhyolite cap at points closer than 100 ft to the surface.

Rays which reached geophones 250 or more feet below the surface travelled in more nearly vertical paths. Again the results are not easy to interpret since the composition (and therefore seismic velocity) changed greatly at a point about 265 ft down the survey hole. If the horizontal and vertical velocities at most points below the shot hole were equal (a question on which no evidence is available from this survey), the vertical velocities at various depths can be computed, and these are plotted in Fig. 6.5. Some of these interval velocities were measured in the nuclear shot. The two detonations are consistent, see Fig. 6.6.

The stress wave from the center of the Rainier explosion travelled vertically to Station 0 and nearly vertically to Stations 1, 10, 11, 12, and 13, the last four on the mesa slope. Average velocities of the first pulse and interval velocities in the deep hole are shown in Table 6.2 and Fig. 6.7. The first interval velocity (4350 fps) in Table 6.2 is consistent with the USGS measurement of 3800 fps for nearly vertical travel at the same point.

Average velocities to the distant stations (5 and 6) were somewhat greater than velocities to the others. Therefore, the seismic ray must have travelled a greater distance through a high-velocity layer to reach these stations. A clue to the location of this high-velocity layer is given in Fig. 6.5 and Table 6.3, and in the graph (Fig. 6.8) of arrival times versus ground range. The fact that all but one of the points on Fig. 6.8 lie on a straight line suggests that the first arrivals travelled along an interface; that is, behaved as captured rays.

TABLE 6.2 SEISMIC VELOCITIES

Station	Slant range, ft	Arrival time, first pulse, msec	Velocity, fps	Interval velocity, fps	Arrival time, first peak, msec	Velocity, fps
0AP	897	146	6140	--	186	4820
1AP	965	158	6110	--	186	5190
2AP	1092	179	6100	--	209	5230
3APA	1266	202	6270	--	226	5600
4AP	1538	245	6280	--	281	5470
5AP	2014	296	6800	--	356	5660
6AP	2515	357	7050	--	420	5990
0AP	897	146	6140	4350	186	4820
100	797	123	6480	6080	148	5390
180	718	110	6530	7670	130	5520
250	649	101	6430	5830	118	5500
320	579	89	6510	--	106	5460
10	795	146	5440	--	171	4650
11	857	146	5870	--	169	5070
12	1080	173	6240	--	213	5070
13	1768	275	6430	--	324	5460

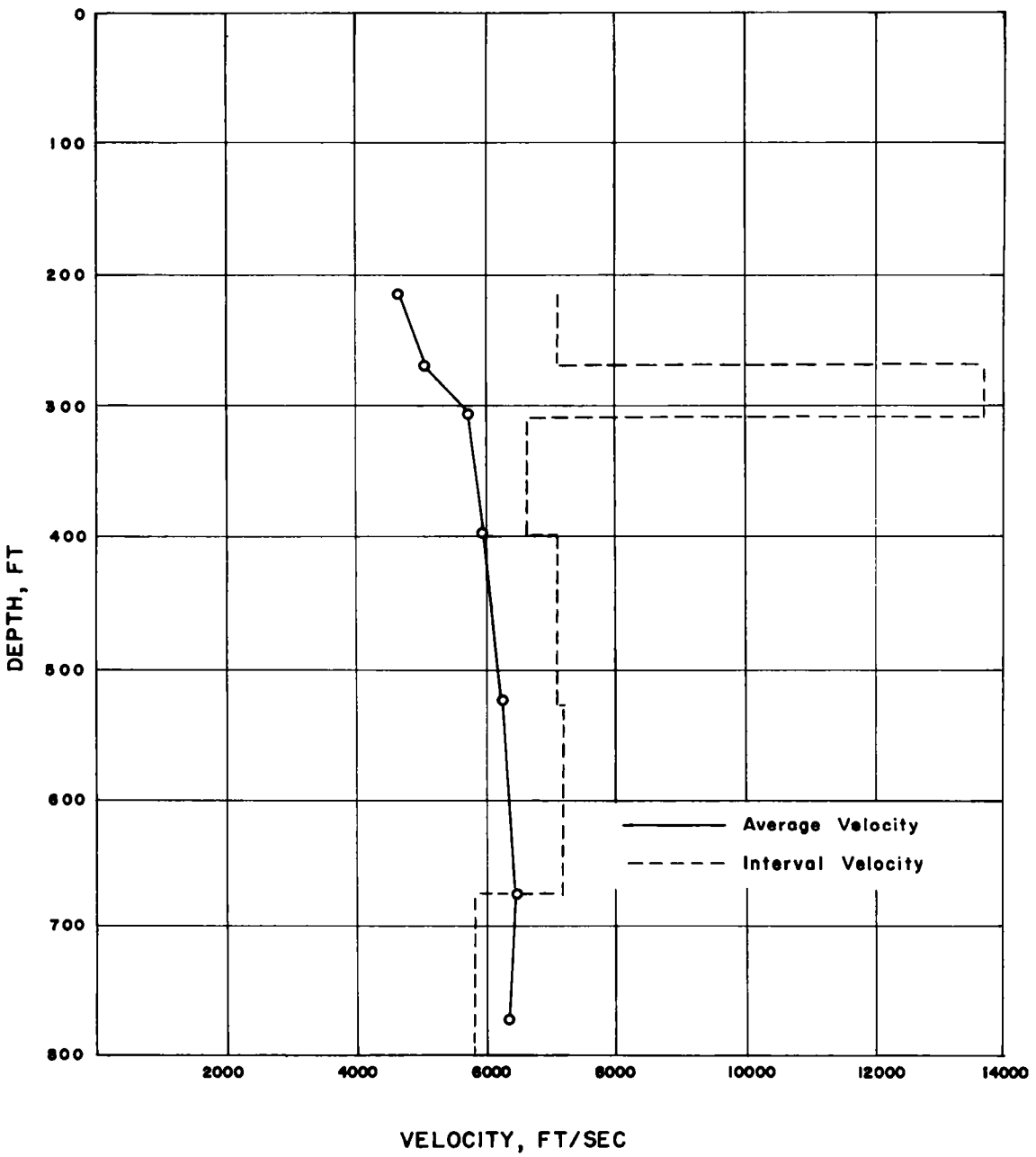

Fig. 6.5 Velocity vs depth, USGS seismic curvey

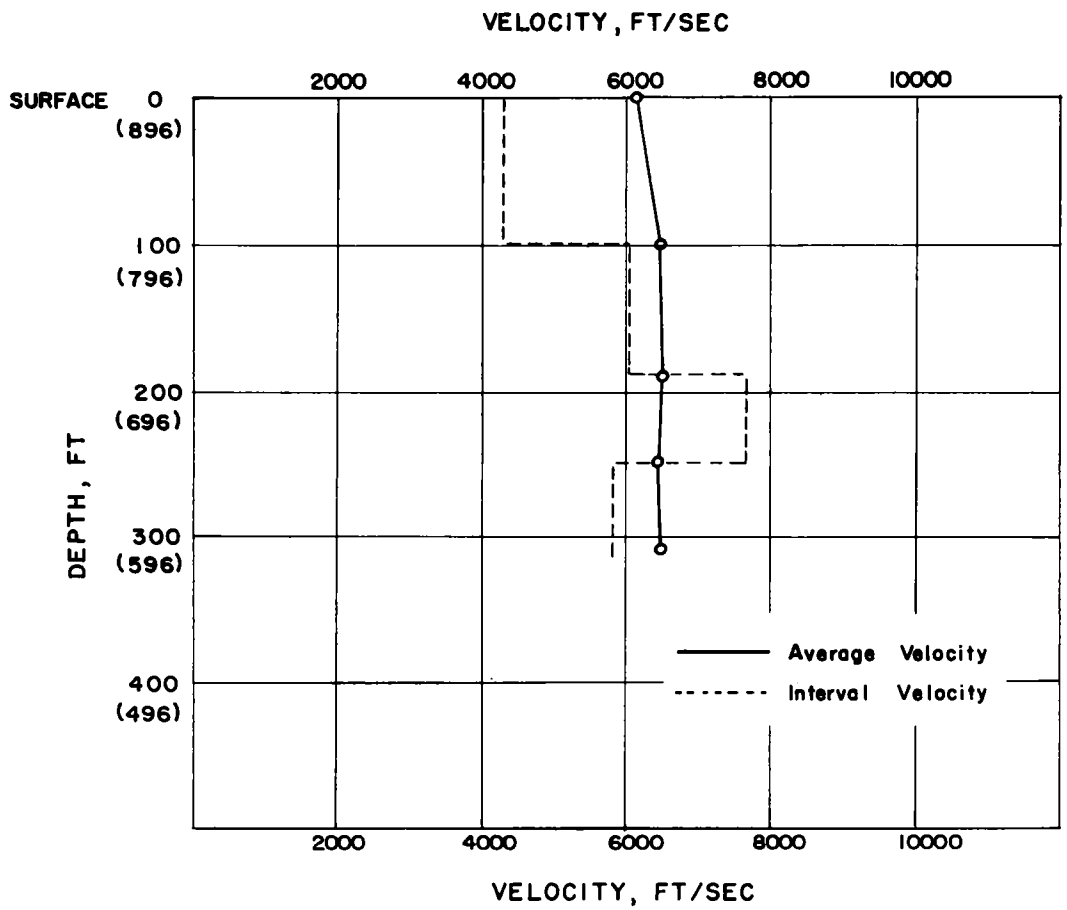

Fig. 6.6 Velocity vs depth, station 0, Rainier shot.

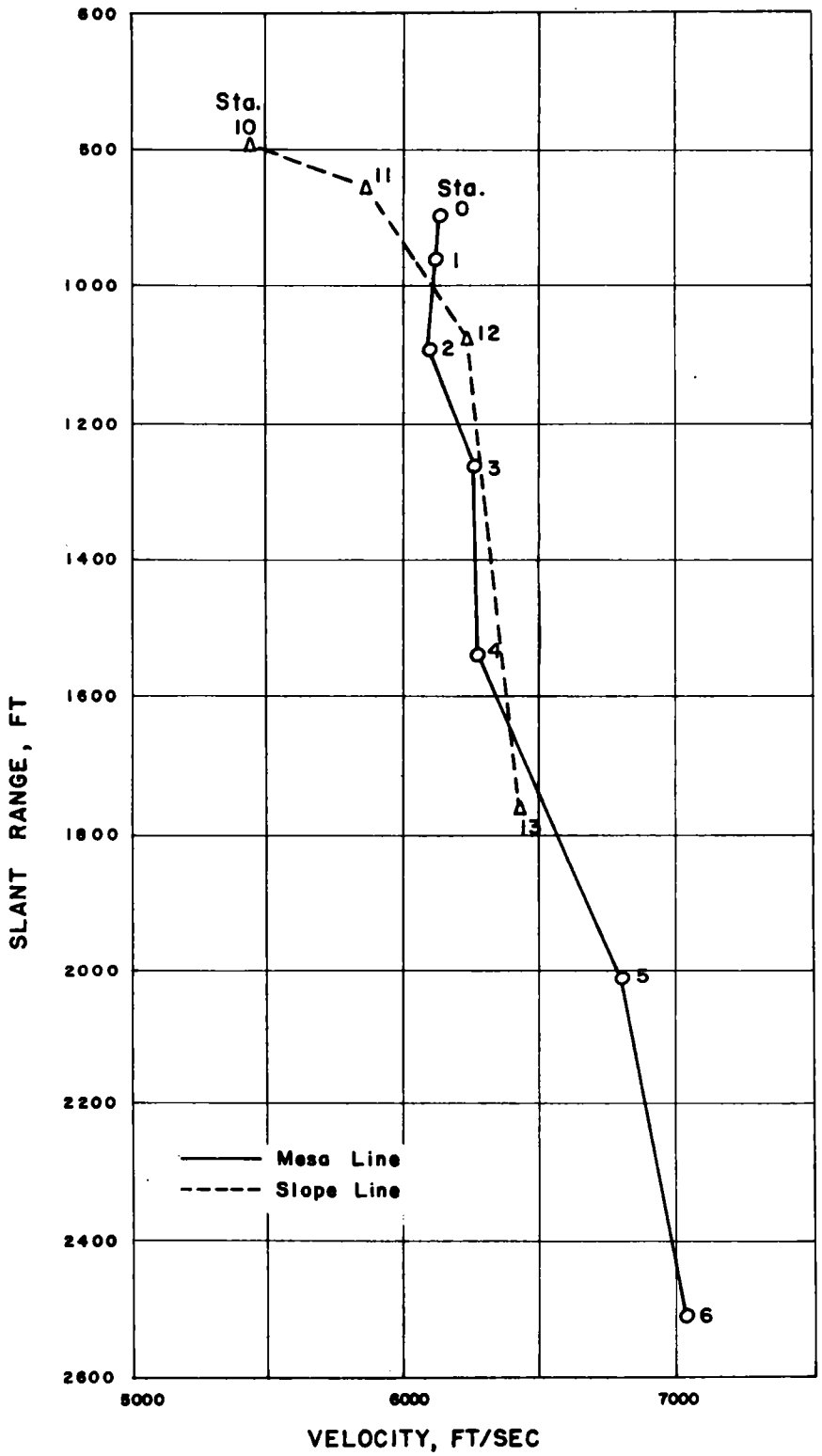

Fig. 6.7 Velocity vs slant range, Rainier shot

To check this idea, rough computations were made as follows. The hill was assumed to be composed of three layers with horizontal interfaces, with seismic velocities and depths as given in Table 6.4.

TABLE 6.3 INTERVAL VELOCITIES FROM USGS DATA

Depth, ft	Interval velocity, fps
230-270	7150
270-310	13700
310-395	6650
395-525	7070
525-675	7180
675-775	5850

TABLE 6.4 ASSUMED VELOCITY PROFILE FOR RAINIER MESA

Layer boundaries (below surface), ft	Isotropic velocity, fps
0-200	5000
200-300	10000
300-900	6600

The refracted rays have been traced through the medium; Fig. 6.9 shows their approximate shapes. Arrival times have been computed according to this figure. For a preliminary model, these computed arrival times show satisfactory agreement with the actual ones: Refinement of the assumptions in Table 6.4 could bring better agreement between computed and actual arrival times.

Tentatively, it may be concluded that the medium was many-layered, with seismic velocities which were widely different in the different layers, and which do not increase monotonically with depth, and that rays to stations on the mesa were captured on a high-velocity interface (Fig. 6.8).

The very low horizontal velocity at 100-ft depth in the USGS seismic survey cannot easily be connected with phenomena measured by SRI. It is possible that there was a major geological discontinuity at this depth before the shot; whether this discontinuity was of a type to cause fracture under tension cannot be determined immediately.

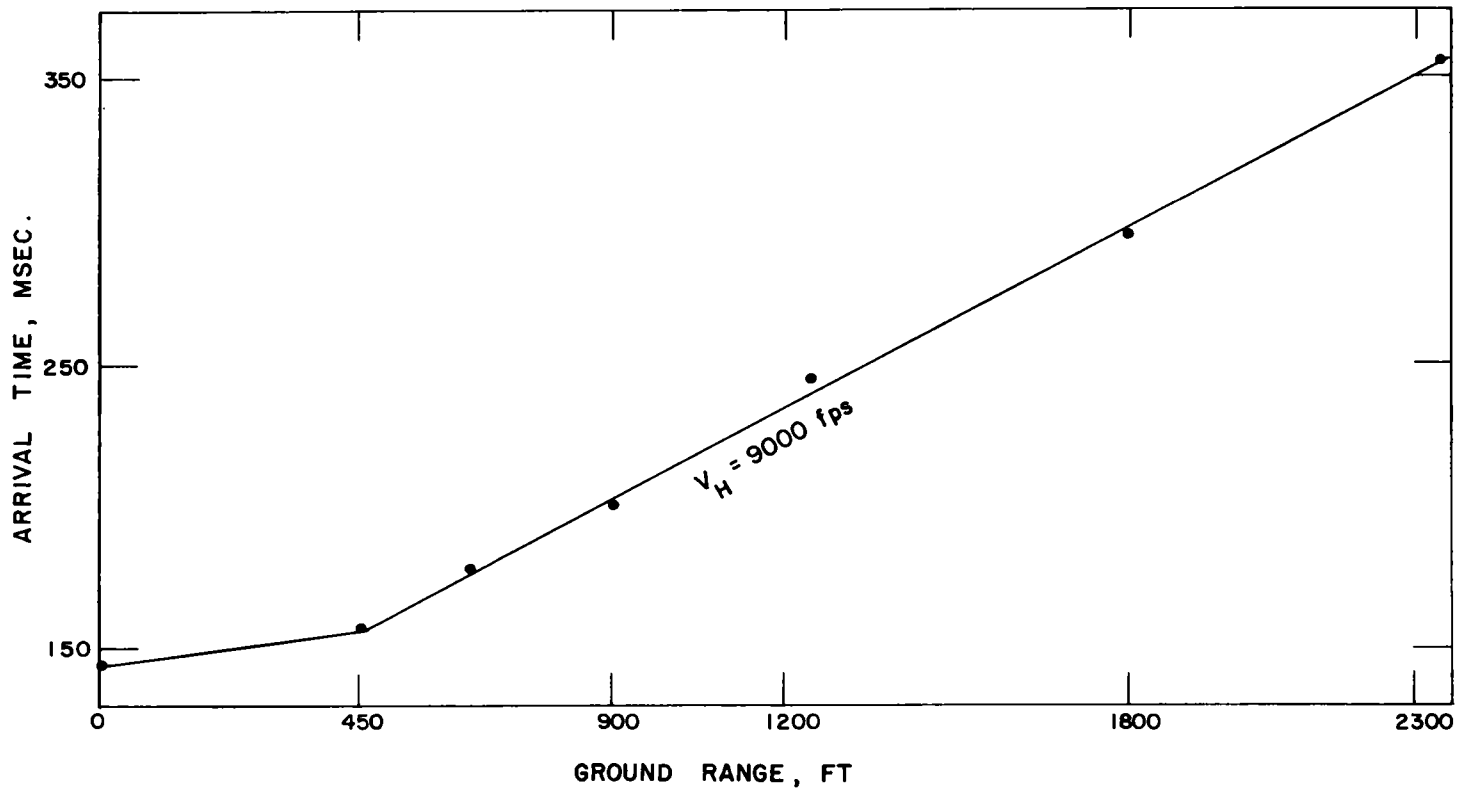

Fig. 6.8 Arrival time vs ground range

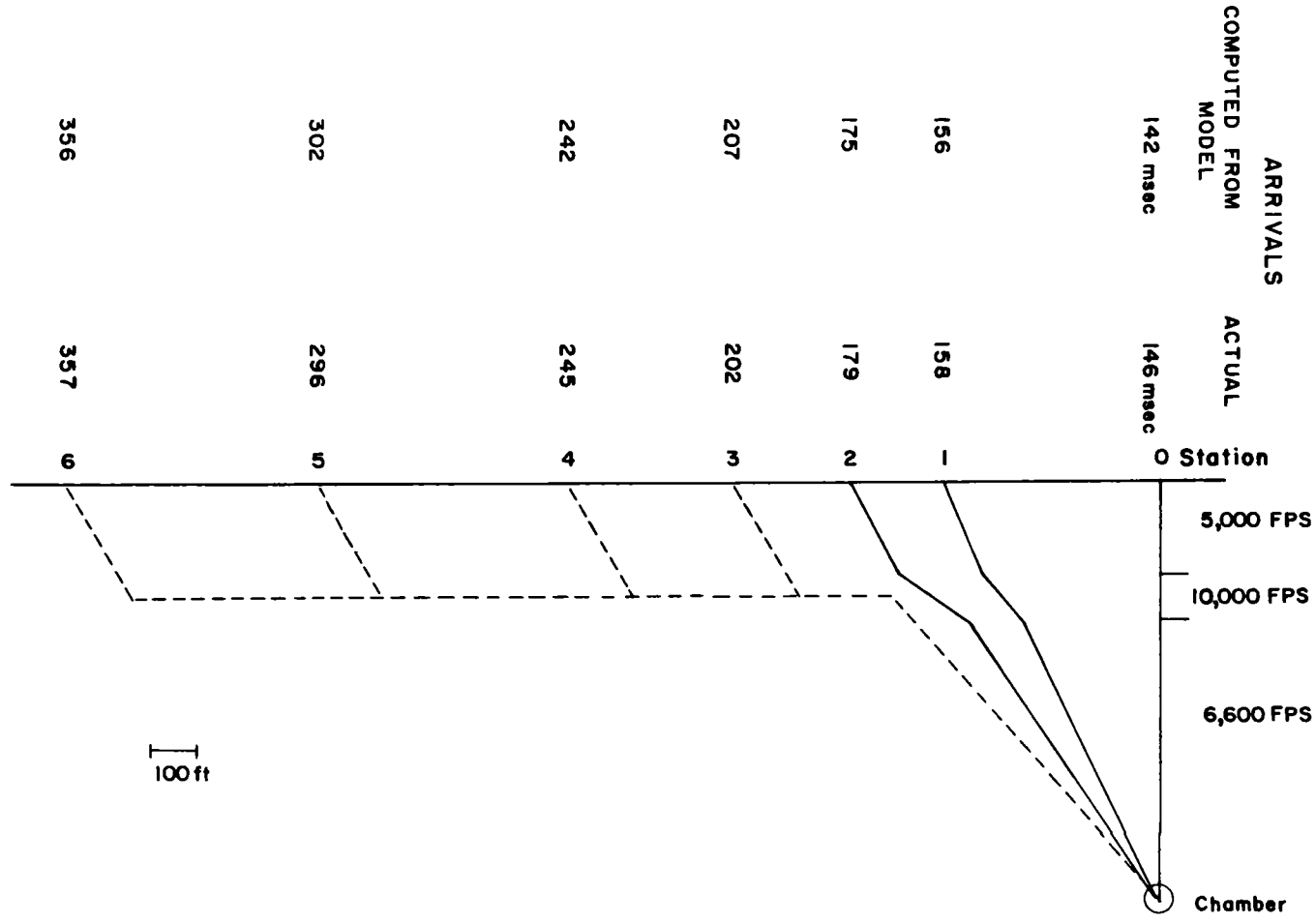

Fig. 6.9 Schematic of seismic rays from chamber

6.4 HORIZONTAL AND TRANSVERSE STRAIN

In general, predicted strains were higher than observations; therefore, most of the strain records are of low amplitude. The most notable exceptions to this are the horizontal strain records obtained on the slope (Stations 10 and 11, Fig. 5.7); these records display large strain maxima occuring after the earth cap had apparently bottomed. Because visual observation at the time of detonation revealed much rock breakage and sliding down the face of the slope, the origin of these large strains on the slope is somewhat in doubt. As a matter of fact, the obvious increase in strain on the 10SH record before the break at 1.04 sec may have been due to a rock hitting the wire span and the strain wire subsequently breaking.

Figure 6.10 is a plot of the first peak horizontal strain versus ground range for the mesa line. Also included on the figure is the shape of the strain prediction curve (normalized to the measured strain at Station 0). It is noted that the horizontal strain measurements, consistent with the acceleration results, indicate that the principal disturbance at the mesa surface was confined to a relatively small (less than 500-ft radius) region surrounding ground zero. Although the shape of the prediction curve is not unlike the observed curve, the latter appears to indicate zero strain at a closer range. The residual horizontal strain data shown in Fig. 6.10 indicate positive strains out to 900-ft radius and near-zero strains beyond. These measurements can best be evaluated when the surface permanent displacement data become available.

As pointed out in Chapter 2, the transverse (0ST) and horizontal (0SH) strain gages at Station 0 were laid out with a common reference point near ground zero; thus, in truth, both gages measured the radial component of strain. Comparison of the maximum positive strains on the two records (Fig. 5.6) shows 3.34 ppk for 0SH and 4.35 ppk for 0ST; this difference, if one assumes symmetrical motion radially out from ground zero, could be accounted for by a preferential motion of the reference point of only 0.45 inch along the 0SH radial direction. Nevertheless, a scatter of this magnitude is not surprising when one considers that several cracks appeared on the surface within the span of each of these gages. The rock simply would not support tensile strains of this magnitude.

Using the data shown in Fig. 6.3, it is possible to compute average earth strains at various depths in the deep hole by observation of the differences in displacement at the same time for two adjacent depths and dividing by the depth difference. The results of this computation are listed in Table 6.5; the average vertical strains are all computed at 0.200 sec, which is before the estimated time of parting of the earth cap from the hill. The computations show that between 320- and 250-ft depth the average strain was 2.7 ppk compressive (negative), while between 250 and 180 ft it was only 0.5 ppk; it is significant that the former strain is in tuff and the latter probably in rhyolite. Moreover, the strain between 180- and 100-ft depth became tensile (positive) and exceeds 3 ppk. This calculation is so approximate that the values presented provide order-of-magnitude data only; however, it is worthwhile for this reason alone.

TABLE 6.5 COMPUTED VERTICAL STRAIN IN DEEP HOLE, SHOT RAINIER

Station No. and Gage code	Depth of gage, ft	Time of displacement, sec	Displacement, ft	Change in displacement, ft	Span, ft	Strain, ppk
0AP320	320	0.200	0.29			
				0.19	70	- 2.7
0AP250	250	0.200	0.10			
				0.035	70	- 0.5
0AP180	180	0.200	0.065			
				0.255	80	+ 3.2
0AP100	100	0.200	0.32			

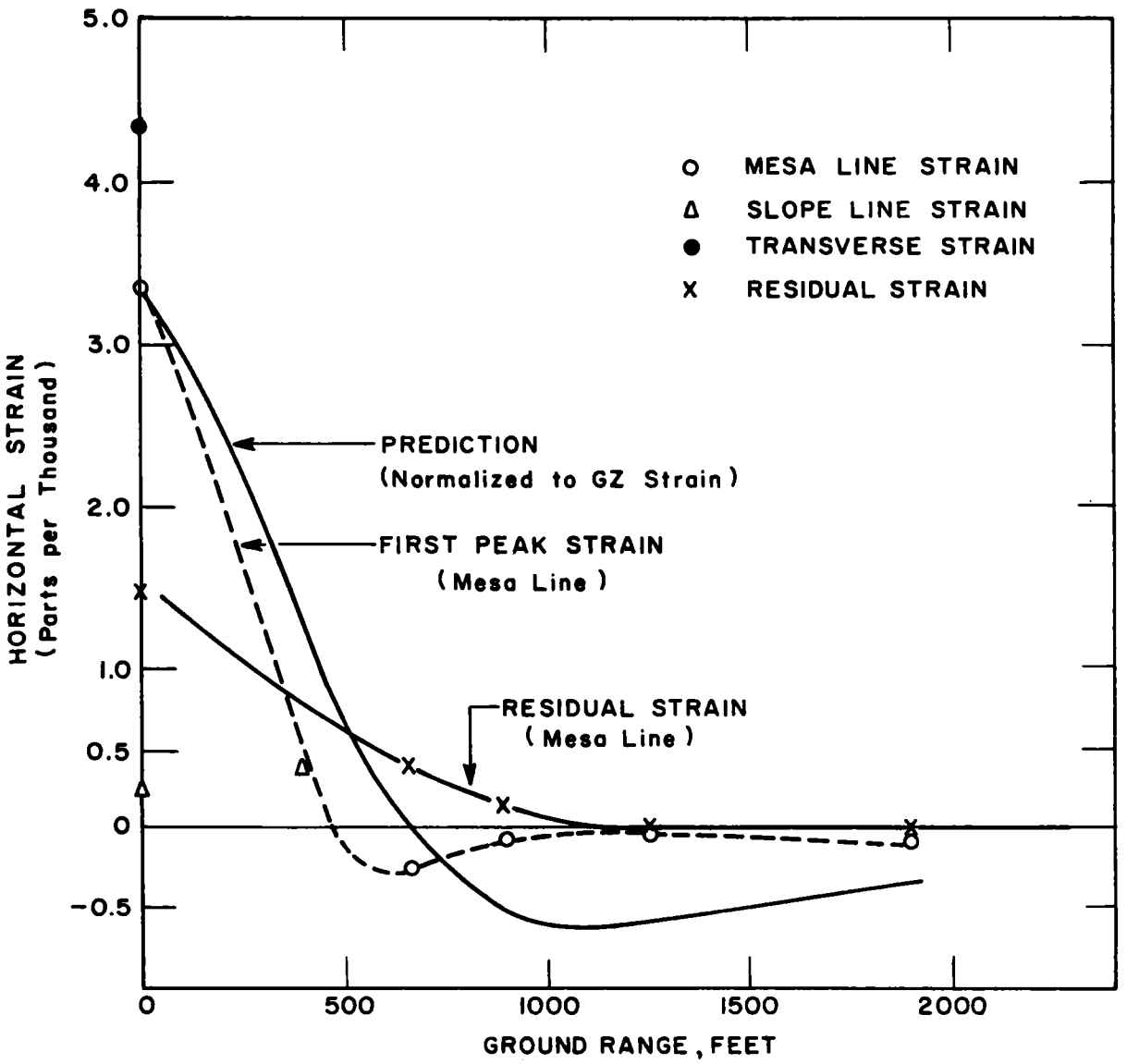

Fig. 6.10 Horizontal earth strain vs ground range, Rainier shot

CHAPTER 7

CONCLUSIONS

The conclusions from a preliminary analysis of data from Project 26.4a can be summarized as follows:

1. Vertical earth acceleration records in the deep hole over the charge indicate that a serious fracture occurred along a horizontal bedding plane between 100 and 180 ft from the top surface of the mesa.

2. Acceleration records on the surface and slope at the mesa confirm the conclusion that a large earth cap separated from the mesa over the charge and subsequently fell back into place. Evidence is available to support the fact that motion was most violent at gage stations located along the mesa slope.

3. Integration of the acceleration-time records to obtain earth velocity and displacement corroborates the earth fracture hypothesis; also, the vertical elevation contours as a function of time indicate that the only significant vertical displacement of the hill occurred at or near ground zero. The maximum vertical displacement on the mesa top was approximately one foot.

4. A careful analysis of the USGS seismic survey data indicates that a layer of high seismic velocity exists at a depth of between 200 and 300 ft below the mesa top. This is substantiated by the gage first arrivals obtained from Shot Rainier which also indicate the existence of other layers of varying seismic velocity. Tentatively, it may be concluded that the medium was many-layered, with seismic velocities which were widely different in the different layers.

5. The horizontal strain measurements, consistent with the acceleration results, indicate that the principal disturbance on the mesa surface was confined to a relatively small region in the vicinity of ground zero. Transverse strains show no consistent behavior.

6. Computations of average vertical earth strains in the deep hole near ground zero substantiate the conclusion that the medium was made up of layers possessing varied physical characteristics.

Future Work. For the final report, some of the tasks to be undertaken are:

(a) Read all records carefully and reduce the data (using the calibration data) on the IBM Model 650 computer.
(b) Integrate, with the electronic computer, the acceleration-time records to obtain particle velocity and displacement.
(c) Correlate the strain data with the permanent displacement survey.
(d) Complete the evaluation of the seismic survey data and the arrival-time data obtained on Shot Rainier.
(e) Correlate SRI results with those of other agencies participating on Shot Rainier.
(f) Summarize the applicability of SRI instrumentation to the motion measurement problem associated with a deep underground nuclear detonation, with a discussion of improvements to be made in such instrumentation.

APPENDIX A

THE MEDIUM OF RAINIER SHOT

According to USGS data, there are in the mesa area three general types of material. Of the total section, about 70% can be classified as typical tuff (volcanic ash), about 15% poorly consolidated tuff, and about 15% welded tuff (rhyolite). In the section above the Rainier charge typical tuff is absent, and welded tuff forms the top 35% of the section.*

The three general types have the following characteristics:†

	Typical tuff	Poor tuff (sand)	Welded tuff (ryholite)
Density	1.57 ± 0.16	1.6 ± 0.2	1.9 ± 0.2
Available porosity, av.	30%	32%	15%
Total porosity, av.	45%	40%	35%
Compressive strength, approx.	8600	2000 (est.)	high
Tensile strength	1000 (est.)	very small	1/9 compressive
Water content	2-10%	15-40%	1-10%

* USGS 10- and 50-ton HE shots were in typical tuff.

† Data supplied by G. V. Keller, USGS.

APPENDIX B

A NOTE ON PREDICTIONS FOR GAGE RANGE SETTING

At a depth h below the plane surface of a semi-infinite elastic medium a spherical bubble of pressure is introduced (see Sketch D). If the radius of the bubble is small with respect to h, then the displacement of the surface at any point M after equilibrium is reached is as follows (from Reference 7).

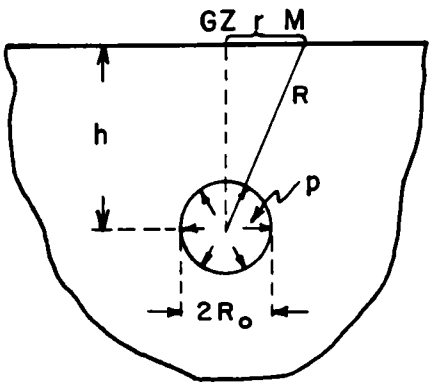

Sketch D

Vertical displacement (at ground-range r) =

$$w = 2(1-\sigma)\frac{C}{Gh^2}\left[1 - \frac{r^2}{h^2}\right]^{-3/2}$$

Radial displacement (at ground-range r) =

$$u_r = \frac{r}{h}\, w \ ,$$

where

σ = Poissons' ratio,

G = Rigidity modulus = $E/2(1-\sigma)$

E = Young's modulus

r = ground range

$C = p\, R_0^3/2$

p = pressure in bubble

R_0 = radius of bubble

For the purpose of predicting ground motion, the true (or dynamic) solution was thought of as a perturbation of the solution of a static problem, in which the explosion center is replaced by a pressure center. In this model, straining but no yielding or fracture is assumed to occur.

There is another approach to the problem of predicting ground motion, which it is proper to mention briefly here. In this other method, each individual particle on the ground surface is assumed to detach itself individually from the medium as soon as the stress wave has been reflected from the surface in the vicinity of that particle. This model is therefore a dynamic one; no doubt it is much more dynamic than it should be. Quantitative results for this model have been obtained in an SRI report (Reference 10). The result

is as follows (Sketch E). If a plane wave is reflected from a surface, the particle velocity at a point P on the surface is about twice the particle velocity in an incident wave (less if the angle of incidence exceeds 80°, or if Poissons' ratio exceeds 0.3). The angle of emergence which the path of a freed particle would make with the original surface is twice the angle which the reflected shear wave makes with the surface.

Since this model was not used for prediction, no specific calculations based on it are included in this report.

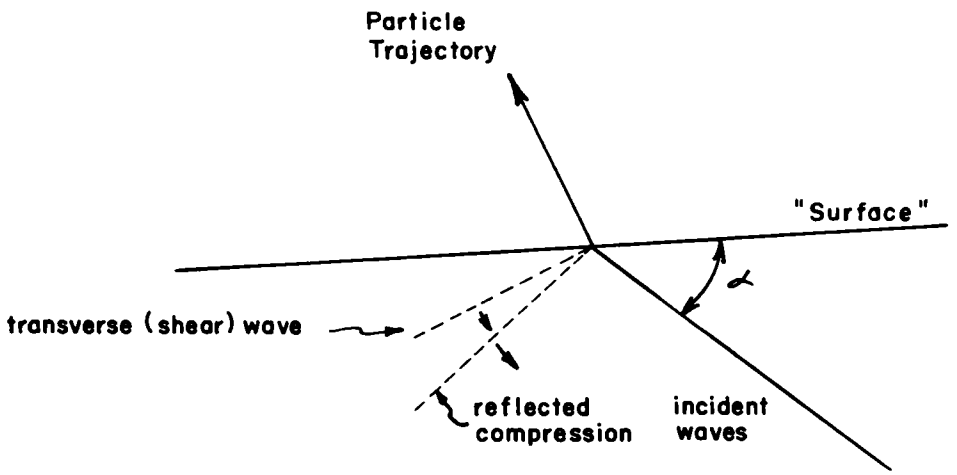

Sketch E. Particle velocity due to reflection of a compression wave at the surface of an elastic medium.

REFERENCES

1. Diment, W. H., and Dobrovolny, E., Feasibility of Proposed Underground Nuclear Test, USGS, 1957.

2. Vaile, R. B. Jr., Crater Survey, Proj. 3.2, SRI, Operation Castle, WT-920, 1955.

3. Engineering Research Associates, Underground Explosion Test Program, TR-5-P-374, Sandstone, Vol. I, Feb. 15, 1953.

4. Doll, E. B. and Salmon, V., Ground Acceleration, Ground and Air Pressures for Underground Tests, Proj. 1.9a, SRI, Operation Buster-Jangle, WT-380, 1952.

5. Swift, L. M. and Sachs, D. C., Underground Explosion Effects, Proj. 1.7, SRI, Operation Teapot, WT-1106[ITR-1106], 1957.

6. Warner, Stanley E., Surface Acceleration Measurements, USGS Tunnel, Room B, NTS, 5 April 1957, UCRL-4913, May 15, 1957. (Operation Plumbbob-Rainier).

7. Carrillo, Report on Subsidence in the Long Beach-San Pedro Area, SRI Report, May 1949.

8. Salmon, V., Air Pressure vs Time, Operation Tumbler, Proj. 1.2, SRI, WT-512, Feb. 1953.

9. Salmon, V. and Horning, S., Earth Acceleration vs Time and Distance, SRI, Operation Tumbler, WT-517, Feb. 1953.

10. Poncelet, E. F., Kats, S., and Fowles, G. R., Fundamental Studies of Small Cratering Charges (Foxhole Charges), SRI, Final report, Vol. II, Feb. 15, 1956.